BOND VALENCE STRUCTURE ANALYSIS OF DOPED BISMUTH SODIUM TITANATE

BY

CONOR JAMES WALSH

A THESIS
SUBMITTED TO THE FACULTY OF

ALFRED UNIVERSITY

IN PARTIAL FULFILLMENT OF THE REQUIREMENTS
FOR THE DEGREE OF

MASTER OF SCIENCE

IN

CERAMIC ENGINEERING

ALFRED, NEW YORK

OCTOBER, 2004

BOND VALENCE STRUCTURAL ANALYSIS OF DOPED BISMUTH SODIUM TITANATE

BY

CONOR JAMES WALSH

B.S. ALFRED UNIVERSITY (2002)

SIGNATURE OF AUTHOR (Signature on file)

APPROVED BY (Signature on file)
WALTER SCHULZE, ADVISOR

(Signature on file)
STEVE PILGRIM, ADVISORY COMMITTEE

(Signature on file)
SCOTT MISTURE, ADVISORY COMMITTEE

(Signature on file)
DOREEN EDWARDS, CHAIR, ORAL THESIS DEFENSE

ACCEPTED BY (Signature on file)
ALASTAIR CORMACK, DEAN,
SCHOOL OF ENGINEERING

ACKNOWLEDGMENTS

I would like to thank Dr. Schulze for his guidance and support during this project. I am grateful that I was able to continue my academic career here at Alfred under the guidance of Dr. Schulze. I would also like to thank Dr. Pilgrim and Dr. Misture for their help and support on this project and for being on my committee.

I would like to thank the following undergraduate students that spent many hours preparing and testing many of the samples that were used for this study: Erik Pavlina, Harlan Brown-Shaklee, Matt Dispenza, Kenny Billings, Geoff Freeman and Erin Hendrick. Without their help this project would not have progressed as quickly as it did.

Thank you to Dr. I. David Brown of McMaster University, Canada and his wife for their hospitality and helpful discussions regarding the bond valence model.

A big thanks to Fran Williams for maintaining all of the equipment in the lab, teaching me how it works, and putting up with all of my questions.

I am thankful for the funding for my research assistantship that was provided by the Defense Threat Reduction Agency contract #TDO039873079.

I would like to thank Sutham for being a great friend and for helping me so much in our 2 years together in the LEC lab.

Nicole, you have been a huge source of strength and encouragement for me over the years. I want to thank you for your support and understanding through the good and bad times. I love you!

Katie, thank you for being such a caring and loving sister. You always know how to make me feel good about myself. I really appreciate the support that you have given me in my life. Love ya!

Mom and Dad, words cannot express the gratitude that I feel for both of you. You have not only shown me the way to success, but you paved the way to make my journey as easy as possible. Your unconditional love and support is more than I could ever ask for. To thank you as much as you deserve would take the rest of my life. All I can say is THANK YOU and I love you very much!

TABLE OF CONTENTS

LIST OF TABLES

LIST OF FIGURES

Page

LIST OF EQUATIONS

ABSTRACT

This study focuses on a lead free, high temperature ceramic capacitor material having the base composition of $(Bi_{0.5}\ Na_{0.5})\ TiO_3$. The goal is to modify this base composition to create a material that has X7R-like dielectric behavior, while maintaining its inherently good high temperature dielectric properties. This will alleviate some circuit design problems, and will create a component that is less susceptible to drastic environmental changes. Areas of interest include aerospace and weapons system applications, motor control, geological down hole drilling equipment and many more. An extensive experimental compositional matrix, along with theoretical modeling, has been investigated to modify the base material to attain the goals set forth.

Additions of Ba^{2+}, Sr^{2+}, Ca^{2+}, Zr^{4+} and Sn^{4+} were investigated by the bond valence method and dielectric constant measurements. Strontium and tin additions were also studied using the Rietveld refinement method. Many other additions were made to the structure to study the modification of the dielectric response. Both single and multi-component dopant systems were studied to try and create a material that would meet the goal of the project.

Barium additions in bismuth sodium titanate (BNT) raised the value of relative permittivity and lowered the peak temperature to a minimum of 150˚C. Strontium additions raised the relative permittivity value and lowered the peak temperature, while tin additions suppressed the peak relative permittivity and maintained a constant peak temperature. Both additions increased the lattice parameters as predicted by the bond valence method and shown experimentally by the Rietveld refinements. Calcium additions resulted in a decrease in Curie temperature. Calcium is a very small cation that has been found to substitute for B-site cations in some situations. This occurrence is difficult to determine, however the electrical behavior of the calcium doped system may give some insight to this problem. Zirconium additions up to about 5 mol % increased the shoulder in the curve near 200° C. Above this percentage, the peak relative permittivity was suppressed similarly to the tin doped system. The multi-component systems that were studied exhibited results that combined the behavior of each of the

individual components. This trend, along with the bond valence modeling was used to guide the direction of the project.

The bond valence method was used to compare the measured and calculated lattice parameters for the strontium and tin doped samples. The results show that the theoretical calculations are within a few hundredths of an angstrom of the measured lattice parameters for the samples. This can be useful to calculate how the size of the unit cell will be modified by adding various dopants and for tolerance factor calculations. The tolerance factor calculations are useful for determining compositions to test the electrical properties of. From the tolerance factor calculations, a range has been determined that describes the composition level of morphotropic phase boundary compositions in bismuth sodium titanate.

I INTRODUCTION

A. Bismuth Sodium Titanate

The Bismuth Sodium Titanate (BNT) family of dielectric materials is a relatively new family of dielectrics. It is being studied because of its high temperature dielectric constant, as well as its ability to work well without the addition of lead.[1] BNT is a candidate material for future dielectric and piezoelectric applications that cover large temperature ranges. The large temperature range is advantageous for use in the oil and natural gas industry for down-hole drilling tools, automotive, aerospace and military for applications directly on or near hot engine surfaces. BNT is being studied to create a material that could some day replace the current industry standard, barium titanate.

Barium titanate (BT) is currently the most widely used dielectric material for capacitors. The various dopants that are available for the modification of BT make it the material of choice for many dielectric applications. The downside of BT is that the Curie temperature (T_c) is only 130° C without the addition of lead. Lead additions increase the Curie temperature up to about 150° C; however, lead also de-stabilizes the low temperature phase transitions. Above the T_c, the dielectric constant exhibits Curie-Weiss behavior. The Curie-Weiss law, given by Equation 1, describes the rapid decrease in relative permittivity above the Curie temperature.[2] The drastic drop in relative permittivity beyond the Curie temperature limits the design parameters of ferroelectrics for use in high temperature applications.[3]

$$\varepsilon_r = \frac{C}{T - T_0} \tag{1}$$

Where: C is a constant for a given material (Curie Constant).

T_0 is a temperature near, but lower than the Curie Weiss temperature.

1. Bismuth Sodium Titanate Structure

Bismuth sodium titanate is an ABO_3 distorted perovskite with an rhombohedral R3c crystal structure at room temperature.[4] The standard ABO_3 perovskite formula for BNT is $(Bi_{0.5}\ Na_{0.5})\ TiO_3$. An ABO_3 perovskite can be considered in two ways; one way

is to have the bismuth and sodium cations occupy the corners of a cubic unit cell, oxygen cations occupying the face centers, and a titanium cation in the center of the oxygen octahedra that is formed. The other way, is a three-dimensional cubic network of 8 corner-sharing TiO_6 octahedra with bismuth and sodium cations at the center of the cube formed by the octahedra.[5] Figure 1 represents a typical ABO_3 perovskite, shown here as cubic BNT. The figure suggests that the bismuth and sodium ions are ordered on the A-site of the structure; this is only to show the stoichiometry that is present in an ideal mixture. The real material does not exhibit any long range ordering as described later in the text.

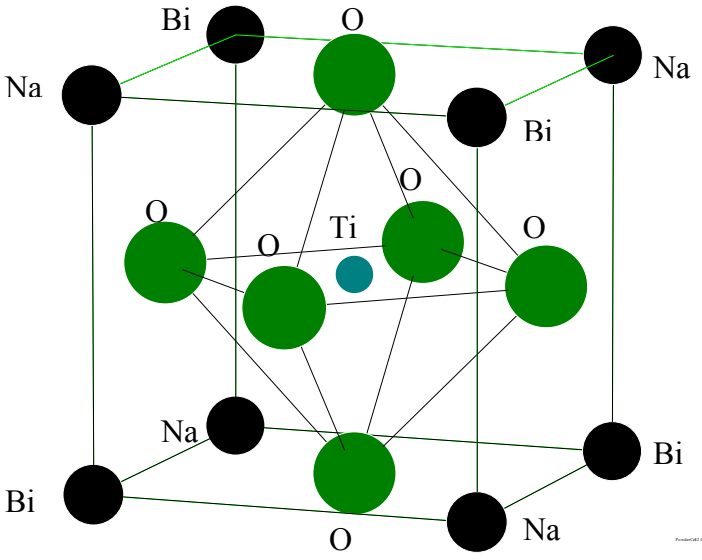

Figure 1: Representation of an ABO_3 perovskite shown as cubic BNT.

Many structural investigations have been performed on BNT since it was discovered in 1960 by Smolenskii et al. These studies used the best methods of the time to determine the phases and phase transitions of BNT.[3,6-11] Phase transitions determined from these earlier studies have since been clarified by an extensive neutron powder diffraction study of BNT. This study definitively determined the phase transitions and crystal structures at various temperatures (Jones and Thomas, 2002). The results of this study are shown in Table I. As the table shows, with decreasing temperature, BNT transforms from cubic Pm3m to tetragonal P4bm and then to rhombohedral R3c with coexistence regions between them. These phase transitions are important to the electrical

properties of the material because only non-centrosymmetric space groups can exhibit ferroelectricity.

The rhombohedral R3c space group is polar with parallel cation displacements along the $[111]_p$ pseudocubic direction along with antiphase $a^-a^-a^-$ oxygen octahedral rotations. Thorough explanations of the types of octahedral tilting and the associated mechanisms are available to more fully understand this phenomenon (Woodward 1997).[5,12] Cation displacements along with octahedral rotations allow the crystal to have a spontaneous polarization (P_s); polarization is necessary for a material to be ferroelectrically active.

The tetragonal P4bm phase is also a polar phase, although it has a weaker polarization response than the R3c phase. The oxygen octahedra in the tetragonal phase exhibits $a^0a^0a^-$ rotation behavior about the c axis with anti-parallel cation displacements of A-site cations along the polar c-axis.[4,13] The tetragonal phase distortion produces a weaker polarization response because the atomic displacements are less than those in the R3c phase. Smaller atomic displacements result in a lower polarization in the material. This is evident by the decrease in relative permittivity above the Curie temperature (320˚C).

Table I: Phase Transitions in BNT Measured by Jones and Thomas, 2002.

Temperature (°C)	Phase(s)	Lattice Parameters (angstroms)	Glazer Tilt System
-268 to 255	Rhombohedral – R3c	$a_H = 5.4887$ (2) $c_H = 13.5048$	$a^-a^-a^-$
255 to 400	Coexisting Rhombohedral/Tetragonal	Variable	Mixture
400 to 500	Tetragonal – P4bm	$a_T = 5.5179$ (2) $c_T = 3.9073$	$a^0a^0a^-$
500 to 540	Coexisting Tetragonal/Cubic	Variable	Mixture
Above 540	Cubic Prototype – Pm3m	$a_C = 3.91368$ (3)	None

Phase transitions in ferroelectric materials are one of the main parameters that need to be controlled to tailor the properties to meet specific applications. Phase transitions are one of the main determinants of the dielectric properties of the material. Compositional additions to the BNT structure can be chosen to modify the phase transitions that occur within the material at various temperatures. Dopants are selected to change specific characteristics of the phases such as relative permittivity, Curie temperature (T_c), relative permittivity peak height and number of phase transitions. The Curie temperature is the temperature where the relative permittivity of the material is the largest. This usually occurs where there is a phase transition. Some materials, such as $BaTiO_3$, exhibit Curie Weiss behavior as discussed before, while others undergo a diffuse phase transition.

Bismuth sodium titanate is a relaxor ferroelectric in the rhombohedral phase and it exhibits diffuse phase transitions between each of the phases. Diffuse phase transitions are described by a coexistence region between phases as discussed above. Diffuse phase transitions are evident in the dielectric response because the relative permittivity peaks become broad instead of having a sharp peak, like those seen in materials with Curie Weiss behavior. Broad relative permittivity peaks are most prominent in solid solutions and in disordered structures. The Curie range, rather than the Curie temperature can be used to describe the broad peaks that are created by the diffuse phase transitions.

The temperature range will typically vary with the frequency used in the measurement. The breadth of the phase transition depends mostly on the amount of disorder in the structure. Largely disordered structures will have a wider peak than those with less disorder. Each compositional fluctuation in the material will exhibit its own peak dielectric constant. These individual units combine together to form a broad peak that is composed of many smaller compositional peaks. If each compositional unit had a peak K at different temperatures, the material peak would extend over the range of temperatures of the individual units. This broad peak can be thought of as a global average of the peaks created by the individual disordered units. The disordered material basically acts like a composite matrix where each section has an effect on the overall properties of the matrix.[14]

2. Dopant Effects in Bismuth Sodium Titanate

Many studies have been performed on BNT to determine how dopants affect the structural and electrical properties of the material. Some studies focus on dielectric properties, while others focus on piezoelectric properties. BNT is a good material for both applications because it can be modified to enhance a specific desirable behavior. Both A-site and B-site dopants have been studied to determine how they affect the properties of BNT, some of these dopants include (Ba, Pb, Sr, Zr, La, K, Bi).[1,3,7,8,10,15-31]

Attfield, 2002 states that the properties of ABO_3 perovskites are mainly controlled by the B-site cations; however, the properties of the material are tuned by the cation(s) on the A-site.[32] This statement is somewhat misleading because the properties can be tuned by both A and B-site doping. The main characteristics of the perovskite must be determined on an individual basis for a more accurate assessment of the ferroelectric properties. Some materials are distorted on the A-site as in BNT, while others such as BT, exhibit B-site distortion. The type of distortion present in the material can be determined by the bond valence method, discussed later in the text. A-site distortion in BNT is created by the valence deficiency of the Bi^{3+} and Na^{+} ions, along with their ionic size compared to the space that is available in the structure.

For many years, the Goldschmidt tolerance factor calculation has been used to determine the stability of perovskites. This calculation, given by Equation 2, only considers ionic size to determine the type of perovskite that will form. This method is limited in its use because it only gives a range of values for which a mixture of ions will form a stable structure. It also gives a vague range that could help to determine if the structure will be ferroelectric (FE) or antiferroelectric (AFE). It does not give any information regarding the type of distortion that will take place in the structure. Over the years, tolerance factor ranges have been determined to describe the typical behavior of a material in that range. On the other hand, the bond valence tolerance factor, discussed later in the text, uses the valence of the ions along with other variables to determine the distortion mechanism of the structure.

$$t = \frac{R_A + R_x}{\sqrt{2}\left(R_B + R_x\right)} \tag{2}$$

Where: R_A is the ionic radii of the A-site cation

R_B is the ionic radii of the B-site cation

R_x is the ionic radii of the anion

The typical range for stable perovskite mixtures is between $0.78 \leq t \leq 1.05$ for VI and XII coordination and Shannon-Prewitt radii.. This range is limited in its predicative value because it has been found that AFEs range from $0.78 \leq t \leq 1.00$, and that FEs can be found throughout the full range.[33] Other tests must be performed to confirm the behavior of the material.

3. Barium Doping in Bismuth Sodium Titanate

The effects of barium on the properties of BNT have been characterized by various groups over the years. Many studies that involve barium doping also include another A or B-site cation to evaluate the effects of multiple-site doping on the properties.[3,15,17-19,23] One of the advantages of doping with barium is that there is a morphotropic phase boundary (MPB) between the rhombohedral and tetragonal phases of the structure. Dielectric materials near an MPB are interesting because they exhibit anomalously large dielectric constant values compared to other compositions. BNT doped with barium has been shown to exhibit an MPB near 7 mol % Ba. The compositions near this value exhibit a large, broad dielectric constant peak. The broad peak is a result of the MPB behavior, along with increased disorder created by the Ba^{2+} ions that substitute for the Bi^{3+} and Na^{+} ions on the A-site. As discussed earlier, diffuse phase transitions present in relaxor ferroelectrics are caused by increased disorder in the structure. Figure 2 shows a phase diagram for a solid solution between BNT and BT with increasing BT mol %.[17]

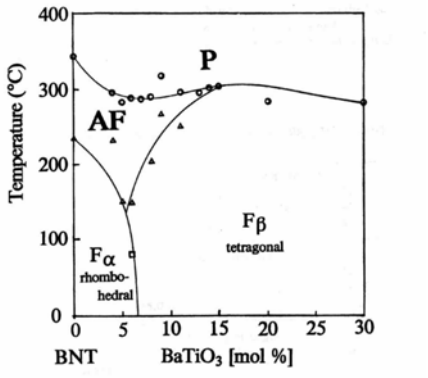

Figure 2. Phase diagram for BNT with increasing mol % BT.[17]

Doping BNT with multiple cations is another way to modify the structure to obtain results that could not otherwise be obtained by single dopant modifications. Sheets et al. simultaneously doped BNT with Ba^{2+} and Zr^{4+} ions to stabilize the AFE phase to near room temperature. This is important because the peak that is created is very broad with a stable relative permittivity over a large temperature range. They also determined that the behavior between single crystal samples, and polycrystalline samples of the same composition were virtually identical; except, the single crystal sample had a larger value of relative permittivity.[15] This behavior is to be expected in a dielectric material because a single crystal is free of defects such as cracks, voids and grain boundary effects that will combine to reduce the overall relative permittivity of a polycrystalline sample.

Li et al. reported that doping with 6 mol % Ba and 1 mol % each of La^{3+}, Co^{3+} or Nb^{5+} will modify the dielectric response compared to BNT doped with 6 mol % Ba. Each of the dopants reduced the value of the relative permittivity and some enhanced the intermediate phase transition referred to as a 'shoulder' in some articles. The addition of La^{3+} also produced smaller grain sizes than the other dopants.[18]

Nagata et al. reported on the properties of BNT with the addition of both $BaTiO_3$ and $(Bi_{0.5}K_{0.5})TiO_3$ (BKT). They reported that an MPB exists at a composition containing 85.2% BNT, 2.8% $BaTiO_3$ and 12% $(Bi_{0.5}\ K_{0.5})\ TiO_3$. Figure 3 shows the phase relationship near the MPB for the BNT/BT/BKT multi-component system. They found that the most useful compositions were located near the MPB because they exhibited the anomalous electrical behavior associated with MPB compositions.[23]

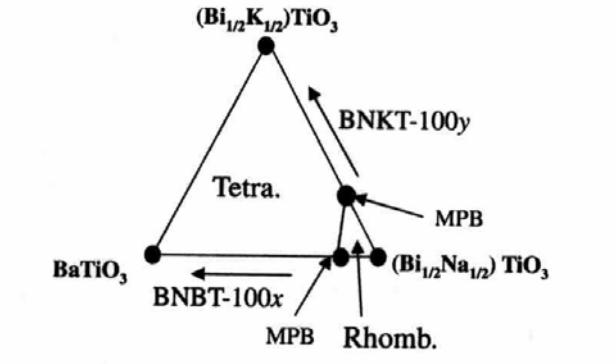

Figure 3. Phase relationship among BNT, BT and BKT near the MPB.[23]

4. Strontium Doping in Bismuth Sodium Titanate

Strontium doping in BNT has a well defined effect on the dielectric properties of the material. Sr^{2+} ions can substitute for both Bi^{3+} and Na^{+} ions on the A-site of the perovskite because the average valence between the Bi and Na ions is 2+. Figure 4 shows a phase diagram created in 1974 for BNT doped with $SrTiO_3$ (ST).[8]

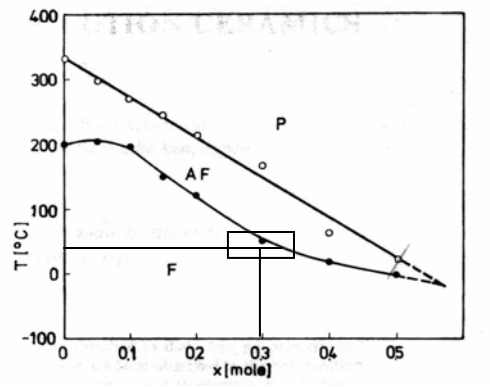

Figure 4. Phase diagram of BNT with increasing strontium doping.[8]

It has been reported that BNT doped with $SrTiO_3$ (ST) exhibits an MPB in the range of 26-30 mol %.[20] The MPB is shown in the phase diagram in Figure 4 above, because there is a tetragonal antiferroelectric region (AFE) between the ferroelectric rhombohedral and paraelectric cubic phases up to about 50 mol % ST. The MPB theory is bolstered by the dielectric measurements because the compositions with 26-30 mol % ST show enhanced dielectric properties with a broad peak, as discussed earlier for MPB behavior. It has been reported that instead of having an MPB, strontium doped BNT exhibits a very large diffuse phase transition region between 26 mol % ST and 50 mol % ST.[7,19] The large temperature range over which the peak K spreads suggests that the diffuse phase transition may be a more reasonable explanation. Park et al. suggests that within the 26-50 mol % region, there are non-uniform units of polarized material within a matrix of non-ploarized material.

To explain this point further, in tetragonal structures there are six possible polarization directions. The polar units in the matrix may adopt any of the six directions unless the material has been poled in a specific direction. Thermal energy causes the polar units to vibrate and therefore not maintain a specific direction. If each polar unit does not have a negative counterpart, the material will have a net polarization in a given

direction. This net polarization is the cause of the weakly polar structure found in the 26-50 mol % region of strontium doped BNT.[34]

In general, as the amount of Sr^{2+} increases, the dielectric constant peak will increase in value, and shift to lower temperatures. Increasing Sr content also decreases the lattice distortion of the material; this behavior is predicted by the bond valence model discussed later in the text. The peak temperature decrease has been shown to decrease in a highly predictable linear manner.[7] Figure 5 shows the linear nature of the decrease in peak temperature of BNT as the amount of strontium is increased. The slope of the line is reported to be -5.3°C/mol%. The linear nature depicted in the figure is advantageous for tuning the peak temperature to a specific value.

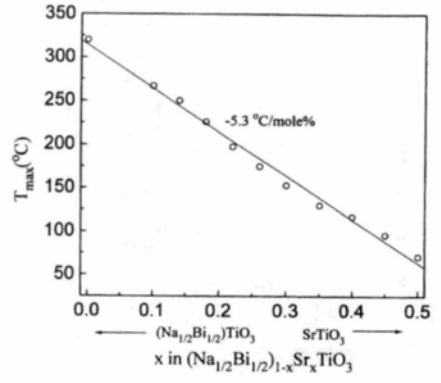

Figure 5. Decrease in T_{max} of BNT with increasing mol % Sr.[7]

5. Doping That Causes Peak Suppression in Bismuth Sodium Titanate

One element that has been used for peak suppression in PZT is tin (Sn^{4+}). Tin is used as a substitute for zirconium or titanium on the B-site in PZT to stabilize the antiferroelectric phase of the material. Feng et al. discovered that as the amount of Sn was increased in PZT, the main dielectric constant peak became more diffuse, and reduced in value along with a slight shift to lower temperatures. Their results for relative permittivity versus temperature showed that the peak temperature reduced slightly and that the peak was suppressed as the amount of tin dopant increased.[35,36]

Nagata et al. discovered that with the addition of $BiScO_3$, the main dielectric peak in BNT will become more diffuse; as a result, peak suppression will occur. Extra bismuth ions were added because it was concluded that the ferroelectricity of BNT was mainly caused by the Bi^{3+} ions on the A-site of the structure. Therefore, they did not

want to remove Bi^{3+} ions by substituting them directly with Sc^{3+} ions. The relative permittivity versus temperature results for these additions showed that as the amount of $BiScO_3$ increased, the permittivity peak was suppressed.[1]

6. Lead Doping in Bismuth Sodium Titanate

The use of lead in electronic ceramic materials has been common over the years because of the good properties that lead provides. The lone pair characteristics associated with lead creates ions that are capable of large polarizations in materials. The large amount of polarization is useful for synthesizing materials with a high permittivity, and a large electromechanical response in piezoelectric materials. The problem with lead is that it is not environmentally friendly; being that it is fairly toxic to living organisms. Special care must be taken when handling lead in its many forms to prevent any contamination of the worker or the environment.

Lead Pb^{2+} doping on the A-site in BNT is useful because it boosts the relative permittivity, and enhances the response of the intermediate phase transition that occurs near 200°C. BNT compositions doped with lead have been reported to exhibit an MPB anywhere between 12-18 mol %.[9,16,21] BNT modified by lead has also been modified on the A-site with dopants like K^+, La^{3+} on the A-site, and on the B-site with Zr^{4+}.[10,21,22,37] The addition of K^+ ions to BNT with lead causes an extension of the intermediate phase, and an increase in the relative permittivity. Lanthanum additions shift all of the phase transitions to lower temperatures and reduce the relative permittivity. BNT doped with Pb^{2+} and Zr^{4+} ions has a more diffuse phase transition, which creates a very broad relative permittivity peak.

7. Other Dopants in Bismuth Sodium Titanate

There are many other elements and combinations of elements that can be used for doping BNT to modify its properties. One such element of interest is lanthanum La^{3+}, because it restricts grain growth and enhances densification.[28] One of the disadvantages is that it decreases the magnitude of relative permittivity at room temperature because it is replacing a more polarizable ion in Bi^{3+}. Lanthanum doping enhances the shoulder that appears near 200°C, and broadens the high temperature peak. The peak broadening has been attributed to increased lattice distortion caused by the strain created when La^{3+} ions

replace Bi^{3+} ions on the A-site of the structure.[29] Herabut and Safari performed x-ray diffraction on the La doped samples to determine the lattice parameters of each sample and to determine the phase of each sample. The authors determined the lattice parameters for La doping levels between 0-6 mol %. They found that a phase transition between rhombohedral and cubic would occur near 2-5 mol % La additions.[27]

Another area of interest for BNT doping is with solid solution compounds containing potassium K^+ ions. Compounds such as $Bi_{0.5}$ $K_{0.5}$ TiO_3 (BKT) and $KNbO_3$ (KN) are of interest because of the MPB behavior that they exhibit. The solid solution of BNT-BKT has been found to have an MPB between the rhombohedral and tetragonal phases in the range of 16-20 mol % BKT.[24] This is significant because of the enhanced electrical properties that MPB compositions exhibit. The solid solution of BNT-KN has been found to contain an MPB between the rhombohedral and orthorhombic phases in the range of 94-97 % KN. These results were determined by Ishii et al. and their results can be found in the literature.[25]

B. Bond Valence Analysis

1. General Bond Valence Theory

The bond valence sums method is used to predict the bonding in inorganic compounds. Bond valences are calculated according to Equation 3.[38]

$$S_{ij} = \exp\frac{\left(R_0 - R_{ij}\right)}{B} \tag{3}$$

Where: S_{ij} is the experimental valence for that bond

R_0 is the length of a bond of unit valence

B is a universal constant equal to 0.37 pm [38]

R_{ij} is the bond length between cations i and j

A comprehensive list of R_0 values can be found in the literature as determined by Brown and Altermatt.[38,39] The R_0 values were determined by using information from the International Crystal Structure Database (ICSD). Equation 3 uses bond distances (R_{ij}) measured by x-ray diffraction to determine the bond valences (S_{ij}) of the bonding cations in the solid. A separate calculation must be made for each bond between cations i and j.

Summing the S_{ij} for each bond gives the bond valence sum for the environment surrounding a cation. The A-site cations are typically coordinated by 12 oxygen anions, therefore; equation 1 must be used 12 separate times to get the S_{ij} for each of the 12 Bi-O bonds for one Bi cation. The same can be done for the B-site, which is coordinated by 6 oxygen anions. The bond valence sums are useful to determine if the environment around an ion is distorted, or if the environment is the correct size for all of the ions. If the sum of the valences do not equal the valence of the cation of interest, the environment is not stable; some type of distortion must occur for the compound to form a stable structure.[38]

The theoretical approach uses the ideal bond valence (s_{ij}), calculated by Equation 4 to substitute for S_{ij} in Equation 3 to calculate the theoretical bond lengths.[38]

$$s_{ij} = \frac{valence}{CN} \tag{4}$$

Where: s_{ij} is the theoretical bond valence

CN is the coordination number of the cation

Valence is the expected valence of the cation

By substituting this value into Equation 3 for (S_{ij}), the theoretical bond lengths (R_{ij}) can be determined. The bond lengths are helpful because as the temperature increases and the structure changes from one phase to another, the bond lengths will change accordingly. The change in bond length can help determine when a new phase becomes present and the temperature that the change occurs. The bond lengths can also be used to calculate the lattice parameters and the tolerance factor, which are discussed later in this paper.

Neutron diffraction can be used along with Rietveld structure refinements to obtain accurate lattice parameters, along with ion positions. The ion positions are important because they can be used to calculate accurate bond valence sums around distorted ion positions. The bond lengths of the distorted structure can be used instead of the ideal values. This data is absolutely necessary to obtain actual ion positions because if x-ray is used, the oxygen positions must be assumed to be at the face centers when calculating the bond lengths from the lattice parameters. Neutron data can show the exact length of each bond to oxygen in the structure because the oxygen anions are

detected by neutron diffraction and not by x-ray diffraction. This method can also be used to study the change lattice strain as dopants are added.

The coordination of the cations can be changed to model a distorted structure. As the distortion increases in the structure, the coordination of some cations can increase or decrease to try and accommodate the increase or decrease in valence. For example, an A site cation in a perovskite that is normally coordinated by 12 oxygen anions may reduce its coordination to 8 by forming 4 short bonds, 4 medium bonds and 4 long bonds with oxygen. Depending on the amount of distortion, the long bonds may be large enough that they no longer contribute to the coordination of the A site cation. Typically, a bond length is only considered a bond if the bond valence is larger than $0.038 \cdot V$, where V is the oxidation state of the cation. If the bond valence is smaller than this value, the coordination number of the A-site cation will be reduced by the number of bonds that do not exceed that value.[40] If the 4 long bonds can be considered as non bonding, the effective coordination of the A-site will be reduced from 12 to 8. As shown in Equation 2, changes in CN will have an effect on the lattice parameters of the structure. Increasing the s_{ij} of a bond will decrease the bond length because there is more atomic valence to distribute across a lower number of bonds. The larger valence causes a greater attraction between the cation and oxygen, which will cause the bond length to shorten.

High temperature x-ray or neutron diffraction can be used to "watch" the phases shift in a material as the transition temperature is exceeded. Phase shifts can be determined by using the d spacing of the cations at varying temperatures. The measured values should show a phase shift from the rhombohedral to the tetragonal phase in ferroelectric BNT because the d-spacing should change. Difficulties are encountered if both phases coexist in the material, or if the phases shift slowly so a coexistence region is created. High temperature bond valence calculations can be made that consider thermal expansion to model the phase shifts in the material.[38,41]

2. Tilting of Oxygen Octahedra

Octahedral tilting plays an important role in both ferroelectricity and stability in perovskite structures. The ferroelectric properties of the R3c crystal structure arise from the parallel cationic displacements along the c-axis. The displacements create a spontaneous polarization in the crystal which is necessary for ferroelectric behavior. The

$a^-a^-a^-$ tilt system creates an environment where the cations can displace to create a polar crystal. The stability of the structure is also affected by the octahedral tilt, as the tilt angle is increased, the lattice strain also increases. The lattice strain can reach a point where the bonds are no longer strong enough to retain the structure. When there is too much strain on the structure, two events may take place. The structure may reduce its symmetry to accommodate the strain, or the structure may break down into its constituent materials. X-ray diffraction can be used after calcination to determine if a perovskite structure has formed, or if the individual starting chemicals are still present.[5,12,42-46]

According to bond valence theory, when oxygen octahedra rotate, the coordination number of the A-site cation can be affected. The octahedral rotations cause some bonds between the A-site and oxygen to lengthen, and some to shorten. If the long bonds become too long they can be considered as a non-bond. If this is the case, the effective coordination number of the A-site cation will be reduced by the number of long bonds. In rhombohedral R3c structures, the octahedra have an $a^-a^-a^-$ type of rotation as described by Woodward.[5,12] This type of rotation means that every octahedra is rotated in the opposite direction of its nearest neighbor. The rotation occurs on the $[111]_p$ pseudocubic direction in the R3c crystal structure. The octahedra rotate because the A-site cations are too small for their coordination environment; this causes the oxygen anions to move in a direction that will more evenly distribute the valence of the A-site cations. As discussed in a later section, the bond valence tolerance factor predicts that the BNT structure will have tilted octahedra because the tolerance factor value is less than 1.0.[38]

When oxygen octahedra are tilted, they may also become distorted. A shifting of oxygen anions relative to each other causes the octahedral distortion. However, this is not the case for every octahedron. Howard and Stokes found that only the $a^+a^+c^-$ tilt system in the tetragonal crystal structure was required by geometry to have both tilting and distortion. In the other tilt systems, distortion can be expected, but is not required. Distortion can be expected because the tilting of the octahedra alone may not be enough to satisfy the valence requirements of the cations.[45]

3. Bond Valence Tolerance Factor

The stability of a perovskite structure has been studied by using a tolerance factor calculation to determine whether the structure is possible. The bond valence tolerance factor has been used to determine if a perovskite structure will distort on the B-site or if the octahedra will rotate to accommodate the distortion on the A site. The tolerance factor given by Equation 5, is simply a ratio of the (a) lattice parameter determined from the ideal A-O bond length divided by the (a) lattice parameter determined from the ideal B-O bond length.[47]

$$t = a_{(A-O)} \Big/ a_{(B-O)} \tag{5}$$

The theoretical bond lengths can be calculated by substituting s_{ij} from Equation 4 for S_{ij} and solving Equation 3 for R_{ij}. Experimental bond lengths can also be measured by neutron diffraction and substituted into Equation 5 to obtain the exact tolerance factor of the structure. Neutron diffraction must be used because the ionic positions, including that of oxygen, must be refined to obtain the exact bond lengths between the cations and oxygen.

The bond valence tolerance factor deviates from the Goldschmidt tolerance factor given by Equation 2, in that the bond lengths are calculated by using the bond valence equation. The Goldschmidt tolerance factor is similar in principle; however, the ionic radii for cations in specific coordination environments are difficult to find for many cations. Many times, only 8-coordinate radii can be found; therefore, the calculation must be made using those radii. The uncertainty in ionic radii creates problems because small changes to the tolerance factor value can cause large changes to the structure. The values used in the bond valence equation on the other hand, have been characterized very well and are believed to be accurate for all coordination environments. For a comparison, the tolerance factor of BNT calculated by the Goldschmidt tolerance factor using the available Shannon and Prewitt radii is 0.945 and the bond valence tolerance factor for BNT is 0.959. The difference between the two is caused by the ionic radii values that are available as discussed earlier. The differences noted here demonstrate why the bond valence tolerance factor is a more robust technique for predicting perovskite behavior.

The distortion behavior of perovskites can be determined by the bond valence tolerance factor as follows. If the ratio is equal to 1.0, as in $SrTiO_3$, the structure will have no distortion and will not have any ferroelectric dipoles. By adding different dopants, the tolerance factor can be shifted above or below the ideal value of 1.0. Most perovskite materials are not as perfectly matched as $SrTiO_3$. For example, $BaTiO_3$ has a calculated tolerance factor value of 1.5, while $CaTiO_3$ has a calculated value of 0.95 and $(Bi_{0.5}\ Na_{0.5})\ TiO_3$ has a value of 0.959. Dopants may be added to these structures to modify the tolerance factor. The resulting dielectric properties of the modified material can be measured and compared to the tolerance factor predictions to try and determine if there is a correlation between the tolerance factor and the dielectric behavior of the material.[47]

The tolerance factor is used to determine which distortion mechanism will be present in the structure. For values of t larger than 1.0, the B cation is typically displaced from the center of the oxygen octahedra. This distortion results in a ferroelectric response, as shown by the $BaTiO_3$ example. Values of t less than 1.0 have distortions emphasizing the A-site cations, in which case, the oxygen octahedra rotate to lengthen and shorten some of the bonds to the A cations as discussed earlier.[47]

4. Polyhedral Volume Ratio: An Alternative to the Tolerance Factor

As discussed above, the bond valence tolerance factor has similarities with the Goldschmidt tolerance factor. The bond valence tolerance factor is a more powerful method for determining the distortion mechanism in a perovskite, rather than determining simply a range of values for which a specific behavior should occur.

Another similar method to the two previously discussed tolerance factors has been described by Noel Thomas in many papers. Thomas' method utilizes the ratio of the polyhedral volume of the A-site cubo-octahedra and the B-site octahedral volume. This ratio is defined by Equation 6. Many more complex equations involving tilt angles and specific crystal structures can be found in the references.[42,44,48-52]

$$Volume\_Ratio = V_A / V_B \tag{6}$$

The volume of the AO_{12} and BO_6 octahedra is mainly controlled by the size of the A and B cations in the structure. Increasing or decreasing the ionic size of the cation will

increase or decrease the volume of the octahedra. Variations in ionic size can be used to control the value of the ratio by adding dopants to the structure. This change will increase or decrease the volume ratio to yield a value that will give the desired results.[52]

The volume ratio method has been compared to the Goldschmidt tolerance factor (described above) and it is expected that any relationship discovered by the tolerance factor should also exist in the volume ratio method.[48] A linear correlation has been discovered by Thomas between the tolerance factor values and the volume ratio values for many different perovskite compositions.[48] One of the main advantages of this method is the relationship between volume ratio and octahedral tilt angle. The literature shows a strong correlation between volume ratio and octahedral tilt angle. A ratio value of 5.0 exhibits a zero tilt angle, while decreasing values result in increasing tilt angle. In order to calculate the polyhedral volumes, it is necessary to have accurate lattice parameters and ionic positions. Once these values are known, they can be used by implementing the method proposed in the literature to determine the volume of each polyhedra.[42,44,48-52]

As discussed earlier, a perovskite with no distortion or polarization will have a non polar cubic structure with both the Goldschmidt and bond valence tolerance factor values equal to 1.0. In the volume ratio calculations, this structure will have a value of 5.0. This means that the A-site cubo-octahedra are exactly 5 times larger than the B-site octahedra. A value of 5.0 requires that there is no octahedral tilting in the structure because the environment around the cations is the ideal size.[48]

The volume ratio has been used to predict the temperature that phase transitions will occur in perovskite materials. This was done by taking experimental structural data for different temperatures, and calculating the ratio as temperature increased. The volume ratio will change with temperature because the AO_{12} octahedra are less rigid than the BO_6 octahedra, which leads to the AO_{12} octahedra having a larger coefficient of thermal expansion (CTE) than the BO_6 octahedra. Upon heating, the AO_{12} octahedra will expand faster than the BO_6 octahedra, and the ratio given in Equation 6 will increase until it reaches the ideal value of 5.0. It has been suggested that once the value reaches 5.0, a structural change in the form of a phase transition should occur. One explanation given for the necessity of a phase transition is that as the tilt angle increases, the oxygen anions become closer to each other. As the oxygen anions reach their minimum ionic separation

distance of approximately 1.41Å, a phase transition must occur to alleviate the forces created by the oxygen-oxygen repulsion. This explanation is used to describe the phase transition seen between rhombohedral and orthorhombic phases as the ratio value decreases from 5.0 in some of the perovskites studied in the research.[52]

Unlike the bond valence tolerance factor, which can be both larger and smaller than 1.0, volume ratio can not increase above 5.0 because a phase transition is predicted at that value. When the perovskite structure has transitioned into the cubic phase, the ratio should remain at 5.0 because the polyhedral volumes should be at their ideal sizes. The examples discussed in the research show the volume ratio calculations for different phases as they approach and surpass the phase transition temperature.

The volume ratio method is a powerful tool to determine tilt angles in distorted perovskites, and has been shown to correlate very well with the Goldschmidt tolerance factor. The advantage of this method over the Goldschmidt tolerance factor is that it can more fully explain the structural phenomenon that occurs in perovskites. The method is stronger because it utilizes more structural data than simply the ionic size of the cations. This method is fairly comparable to the bond valence tolerance factor method as it provides more structural information, and explains more fully the reason for the observed behavior in different structures. The method is, however, more difficult to use as a predictive method, and the calculations are numerous and complex.

II EXPERIMENTAL PROCEDURE

A. Compositional Preparation

Conventional ceramic oxide processing methods were followed to produce the samples for this study. The oxide and carbonate powders were weighed according to their respective stoichiometric proportions, then mixed in Nalgene™ bottles on a ball mill with zirconia media in denatured alcohol (95% ethanol, 5% water) for a period of 12-24 hours. The purpose of ball milling was strictly to create a homogenous mixture of the powders, not to reduce particle size. After mixing, the suspensions were poured into Pyrex dishes and the alcohol was evaporated from the mixture in a fume hood. The dried mixture was calcined at 750˚C for 2 hours at a rate of 300 K/hour to burn out the carbonate, and to allow the perovskite structure to form from the individual components. The calcined powders were weighed to determine if all of the carbonate had been expelled from the structure. If the weight was not at the correct amount, the powder was re-calcined at 800°C at the same rate for 2 hours. After calcination, the powder was crushed in a mortar and pestle and a 1% polyvinyl alcohol binder solution was added to the powder in a 1:1 ratio and mixed for 6-8 hours with zirconia media on a ball mill. The milling media were used to break up agglomerates so that the binder could coat as much of the powder as possible. The powder-binder mixture was dried in Pyrex dishes in a fume hood overnight before being ground. The powder-binder mixture was ground with an alumina mortar and pestle and passed through a 100 mesh sieve to ensure uniform distribution of the binder. The grinding step was also used to reduce the particle size of the large particulates that were created during the calcination process below 100 mesh.

Pellets consisting of 2-3 grams of powder were pressed using a laboratory Carver press and a 5/8” die. The pellets were pressed at a minimum pressure of 10,000 pounds per square inch (Psi) to ensure that the powder was well within Stage III compaction.[53] The pressed pellets were fired on a powder bed that consisted of the same powder as the pellets. They were stacked on top of each other with powder placed between them to prevent sticking, and to reduce the chance that volatilization would occur. They were

fired at 1200˚C for 0-2 hours at a rate of 200 K/hour depending on the composition. The geometrical densities of the pellets were measured, and only acceptable if they were above 90% theoretical. If the densities were too low, the firing temperature or time was modified to produce pellets of good density for the various measurements. Geometrical densities were measured, and the theoretical densities were calculated on a weighted average from the data provided by Jones and Thomas 2002. The theoretical density of the materials can be approximated by using Equation 7 below.[29] The volume of the unit cell can be determined from x-ray diffraction, or the volume of un-doped BNT can be used for all calculations to maintain a consistent cell volume. For this study, the cell volume was held constant at the value determined by Jones and Thomas.

$$\rho = \frac{n \times M \times 1.66 \times 10^{-24}}{V} \tag{7}$$

Where: n = the number of ions per unit cell.

M = the molecular weight of the ions constituting one unit cell of the chemical formula.

V = the volume of the unit cell.

The fired pellets for dielectric measurements were electroded with Dupont 7095 silver paste that was fired at 550˚C for 15 min at a rate of 5 K/min. After firing, the electrode surface was polished with a pencil eraser to remove the oxidation layer that forms during the firing cycle. The pellets that were used for x-ray diffraction measurements were wet ground in an alumina mortar and pestle with isopropyl alcohol. Other pellets were retained to perform density measurements and SEM microstructural analysis. The firing profiles described in this section are shown in Figures 39-43 in the appendix.

B. Relative Permittivity Measurements

Dielectric permittivity measurements were performed at high temperature on a Hewlett Packard 4192A LF Impedance analyzer and on a Solatron SI 1260 Impedance/Gain-Phase analyzer. The HP 4192A was connected to a Thermolyne 2100 tube furnace and the Solatron was connected to a Centurion QEX Furnace. Both of the impedance analyzers were connected to a computer running a LabView™ program that

controlled both the temperature of the furnace and the frequency sweep that was used to measure the capacitance and loss tangent. The capacitance and loss tangent were measured on heating from room temperature to 450˚C at a rate of 5 K/min with a 5 minute hold at each temperature to allow the pellet temperature to stabilize. The data points were taken every 10 K to reduce the number of data points. The frequencies were measured at decade frequencies ranging from 100 Hz to 1 MHz.

Low temperature relative permittivity measurements were performed on a Hewlett Packard 4284A precision LCR meter in a front-loading Delta 9039 box chamber connected to a liquid nitrogen tank. The measurements are performed in pseudo 5 terminal mode with four sample holders in the chamber. A Lab View program similar to that used in the high temperature measurements controlled both the frequency and temperature of the measurements. The box furnace was first heated to 200°C at a rate of 10 K/min and held for 15 minutes to remove any atmospheric moisture. The measurements were taken on cooling from 200˚C to -75˚C with data points taken every 5°C, and a cooling rate of 5 K/min, with a 5 minute hold at each temperature to allow the pellet temperature to stabilize. The data from the high and low temperature measurements were combined in plots of relative permittivity vs. temperature to show the dielectric behavior of the various formulations.

C. X-ray Diffraction

X-ray diffraction measurements were performed on a Siemens D500 instrument with a 40 sample changer. The instrument was run at power settings of 40 kv and 30 mA with Cu Kα radiation. The diffractometer was used in Bragg-Brentano geometry with a graphite diffracted beam monochrometer. The powder samples were mounted into a top loaded circular sample holder to be rotated in the instrument at 50 rpm. The rotation of the sample is used to reduce preferred orientation of the crystals. The 2θ ranged from 15˚ to100˚ 2θ, the step size was 0.02˚ 2θ, and the count time at each step was 10 seconds. A hold time of 10 seconds was necessary to increase the signal to noise ratio for the refinements. Divergence slits of 1° were used to increase the resolution of the data. These parameters were chosen to yield high resolution, accurate results with low background for use in Rietveld refinements.[54]

The Rietveld refinements were performed with the GSAS program including the EXPGUI functionality.[55,56] The starting data used for each of the refinements was taken from neutron diffraction work and Rietveld refinements of pure BNT (Jones and Thomas). They performed Rietveld refinements on each phase of the pure BNT material. The x-ray data were refined by using the profile function in GSAS. The refinement was performed according to the guidelines found in a paper written by McClusker et al.[57]

III RESULTS AND DISCUSSION

A. Dielectric Properties

1. $[(Bi_{0.5} Na_{0.5})_{1-x} Ba_x] TiO_3$

Adding dopants to the base BNT material can modify the dielectric properties in various ways to try and create a material with a specific desired response. Barium was added to BNT according to the formula, $[(Bi_{0.5} Na_{0.5})_{1-x} Ba_x] TiO_3$, with x ranging from 0 to 0.5. As shown in the previous formula, barium is an A-site dopant. Figures 6-9 show the dielectric properties of BNT doped with various amounts of barium, along with the loss tangent (δ). As the amount of barium is increased from x=0 to x=0.5, the T_c of the material decreases from approximately 320˚C to 150˚C. Pure barium titanate (BT) has a T_c of 130˚C; therefore, as the amount of barium increases, the T_c of the compound will approach 130˚C. Barium additions also increase the relative permittivity (K) of the material. The permittivity increase is caused by the replacement of Na^+ cations by Ba^{2+} cations that have a larger polarizability. For every Na^+ cation that is replaced by a Ba^{2+} cation, a Bi^{3+} cation must also be replaced to maintain the charge balance between the A and B-sites of the structure.

According to the literature, a morphotropic phase boundary (MPB) exists in Ba doped BNT when x is approximately equal to 0.07. As discussed above, morphotropic phase boundary compositions should exhibit enhanced dielectric properties. Figure 6 shows that x=0.09 Ba exhibits the most enhanced dielectric properties of those near the reported value of x=0.07 Ba. The relative permittivity curves are not necessarily the best method for determining where a MPB is however, because the samples that were measured could have had flaws that would cause the relative permittivity to be lower than expected. There could be problems with the electrode paste or the density of the sample that would cause problems with the measurements. The permittivity data does however support the premise that there is an MPB in the range of $0.05 \leq x \leq 0.1$ Ba. The important information that can be gleaned from the figure

s is that barium doping is a useful for decreasing the T_c of the material and increasing the relative permittivity.

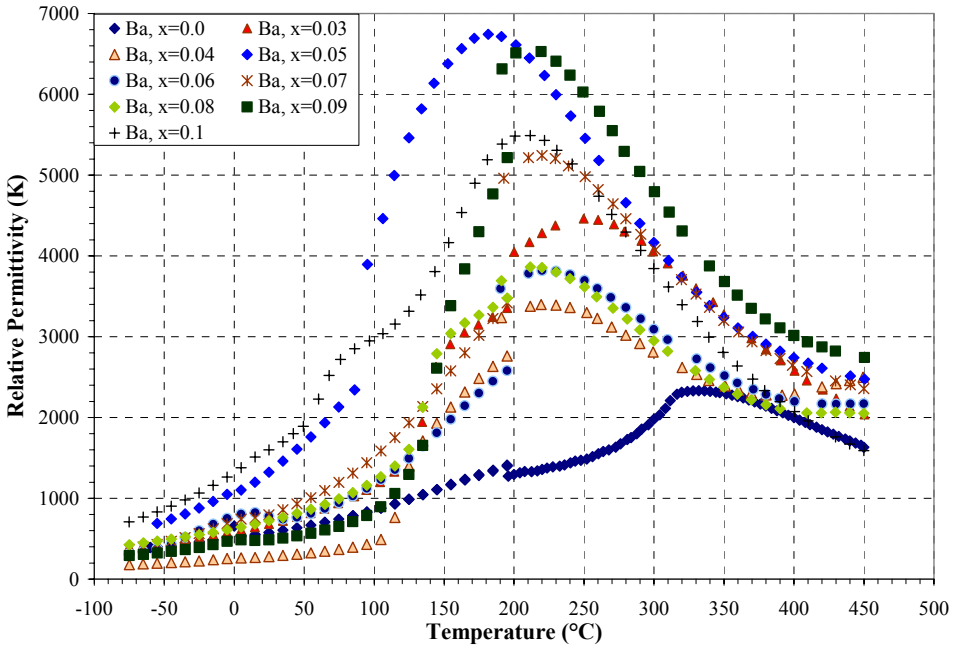

Figure 6. Relative permittivity at 10 kHz versus temperature data for barium doped BNT. Measurements were taken on cooling up to 200°C and on heating from 200°C to 450°C.

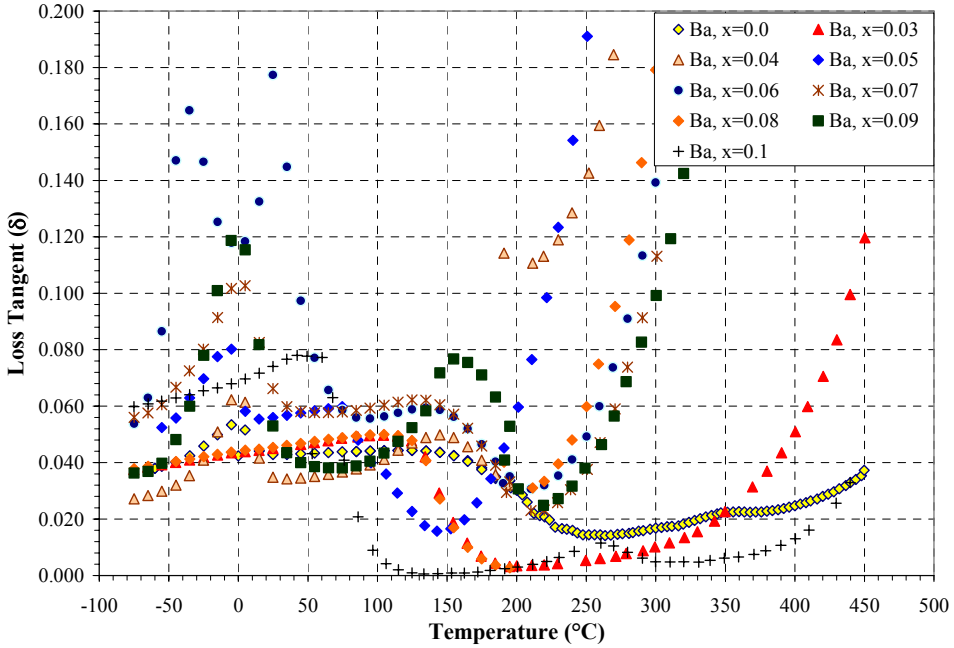

Figure 7: Loss tangent (δ) at 10 kHz versus temperature data for barium doped BNT. Measurements were taken on cooling up to 200°C and on heating from 200°C to 450°C.

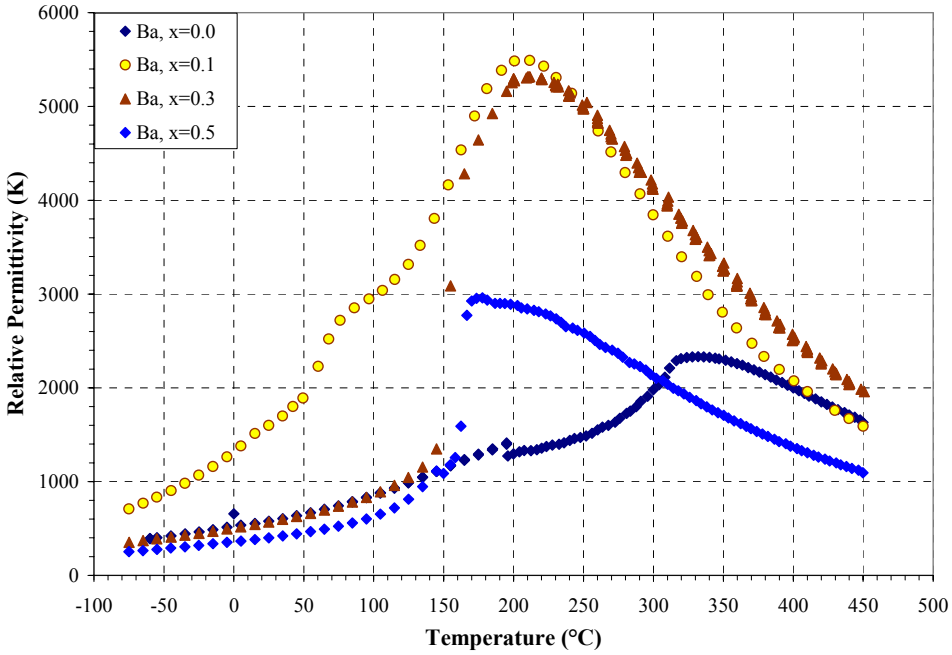

Figure 8: Relative permittivity at 10 kHz versus temperature for barium doped BNT. Measurements were taken on cooling up to 200°C and on heating from 200°C to 450°C.

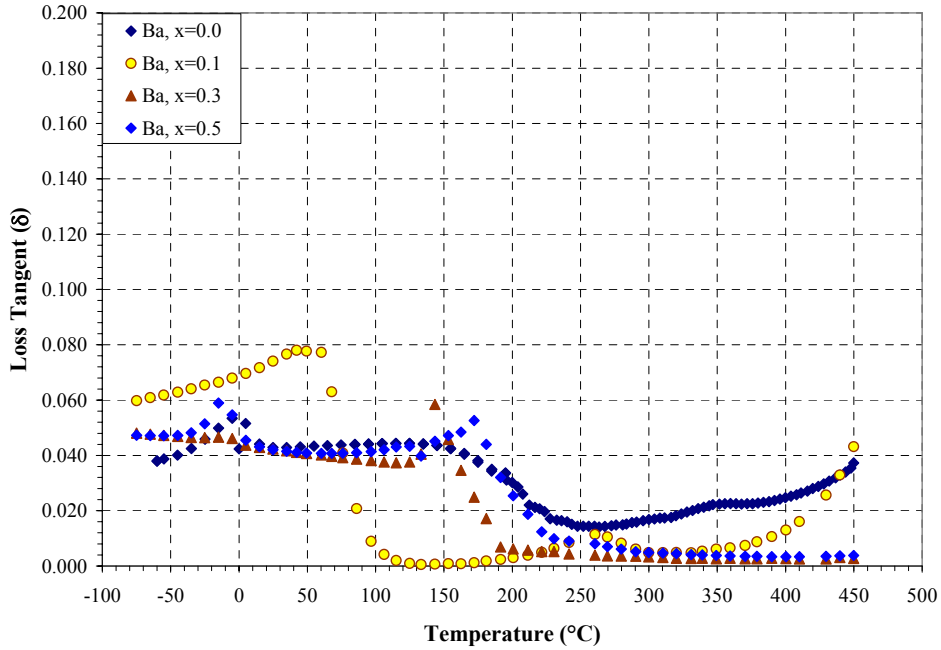

Figure 9: Loss tangent (δ) at 10 kHz versus temperature data for barium doped BNT. Measurements were taken on cooling up to 200°C and on heating from 200°C to 450°C.

2. $[(Bi_{0.5} Na_{0.5})_{1-x} Sr_x] TiO_3$

Strontium was added to BNT according to the formula, $[(Bi_{0.5} Na_{0.5})_{1-x} Sr_x] TiO_3$, with x ranging from 0 to 0.5. Figures 10 and 11 show the relative permittivity versus temperature curves and loss tangent (δ) curves respectively for the strontium doped samples. The results obtained for these samples are comparable to the results published by Park and Hong.[7] As the amount of strontium is increased in BNT, the T_c decreases in a linear manner. Figure 12 shows the peak temperature versus temperature curve as the amount of strontium is increased. The slope of the curve is -5.85°C /mol% which indicates a linear decrease in peak temperature with strontium addition. This result is similar to the findings of Park and Hong whose slope for the same plot was -5.3° C/mol%.[7] The difference in slopes is small, only 0.55˚C/mol%, the variation is because Park and Hong used many more data points which would increase their accuracy. The linear response of peak temperature as the amount of strontium increases is very important because it allows for the prediction of T_c for any composition along the line, without having to measure a sample.

The literature shows that there is an MPB for strontium doped BNT near 27 mol%. The plot of x=0.3 Sr in Figure 10 shows the enhanced dielectric response that is expected for a composition near a MPB. The relative permittivity is much larger for the x=0.3 Sr sample than that of the other samples because of the MPB behavior. The existence of the flat area in the curve indicates a coexistence region where two phases are undergoing a slow phase transition over a large temperature range as discussed above.

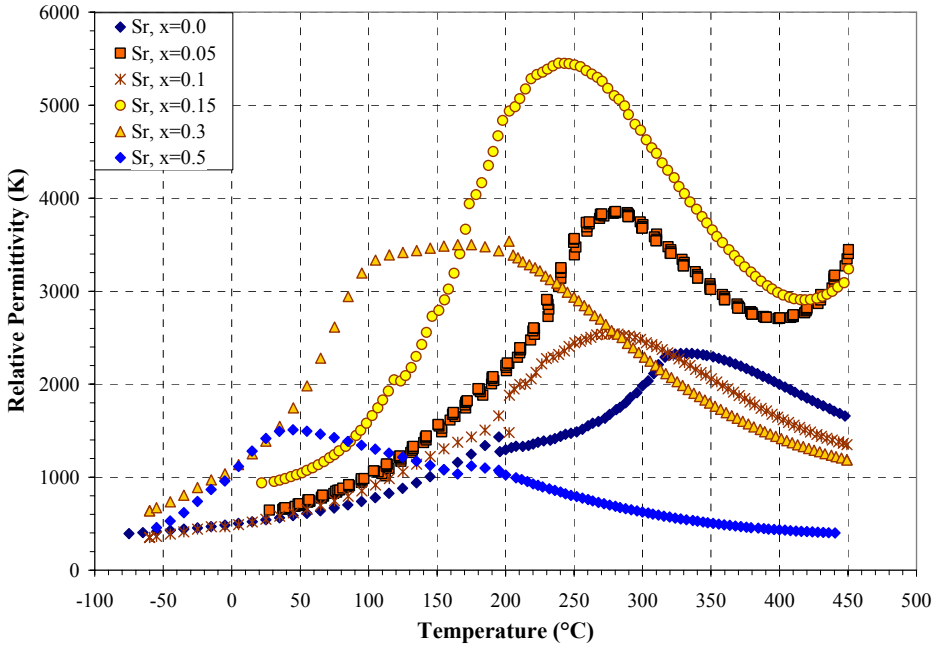

Figure 10: Relative permittivity at 10 kHz versus temperature for strontium doped BNT. Measurements were taken on cooling up to 200°C and on heating from 200°C to 450°C.

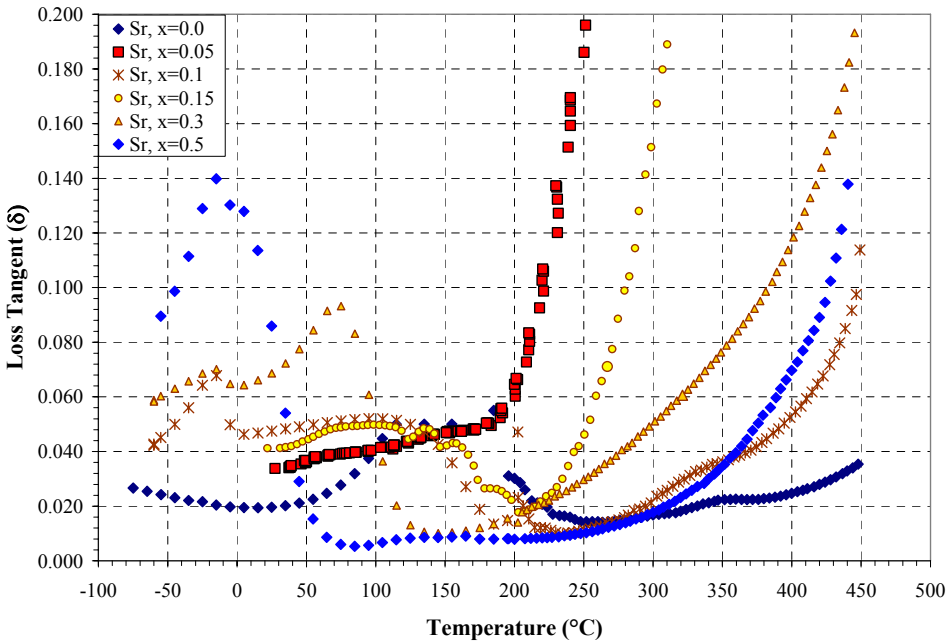

Figure 11: Loss tangent (δ) at 10 kHz versus temperature for strontium doped BNT. Measurements were taken on cooling up to 200°C and on heating from 200°C to 450°C.

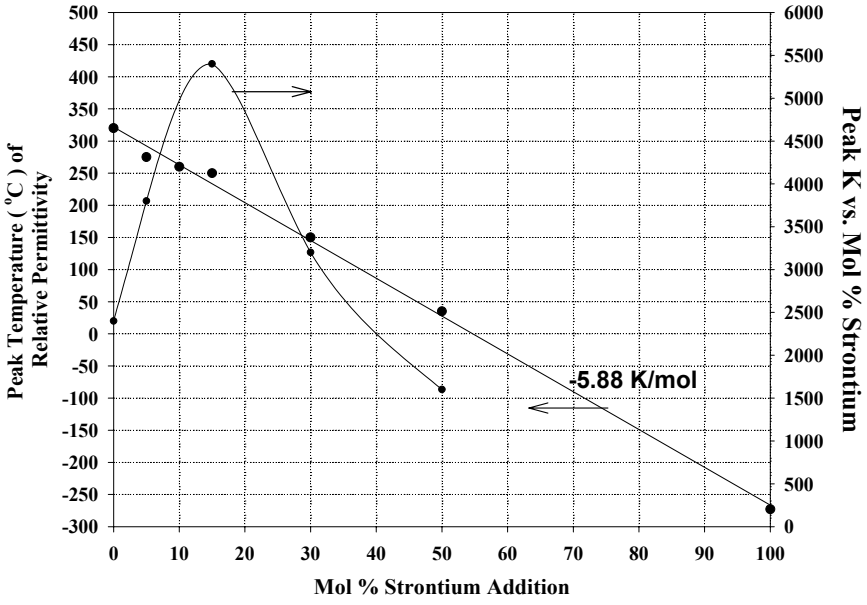

Figure 12: The left hand axis shows peak temperature versus mol % strontium showing the linear response of peak temperature as the amount of strontium is increased. The right hand axis shows the variation in peak K versus mol % strontium.

3. $[(Bi_{0.5} Na_{0.5})_{1-x} Ca_x] TiO_3$

Calcium (Ca^{2+}) was added to the structure according to the following stoichiometric formula, $[(Bi_{0.5} Na_{0.5})_{1-x} Ca_x] TiO_3$ with x ranging from 0.0 to 0.3. Ca^{2+} substitutes for both Bi^{3+} and Na^{+} on the A-site of the structure because the average valence of the two cations is 2+. In barium titanate, calcium has been found to substitute for titanium on the B-site when there is a slight excess of A-site cations. The substitution formula given above was used to restrict calcium from substituting for titanium by creating an environment where only A-site substitution would be favorable.

Calcium substitution in BNT caused a drastic decrease in peak temperature and a decrease in relative permittivity. Figures 13 and 14 show the relative permittivity (K) and loss tangent (δ) versus temperature as the amount of calcium is increased. So far in the study of BNT, the low temperature (less than 0˚C) relative permittivity has been the toughest to modify because all of the curves drop drastically below 1000 at room temperature. The drastic decrease in peak temperature caused by calcium addition is a favorable response because at a level of x =0.15, the relative permittivity is near 800 at

-55˚C. This is approximately 2.5 times larger than BNT and most of the other materials that have been tested so far. The increase in relative permittivity at –55˚C is important because the goal of the project is to create a material with a relative permittivity of at least 1000 over a temperature range of –55˚C to at least 200˚C. Although the relative permittivity is not 1000 as desired, a large step has been made toward discovering a material that will modify BNT to meet the required specifications.

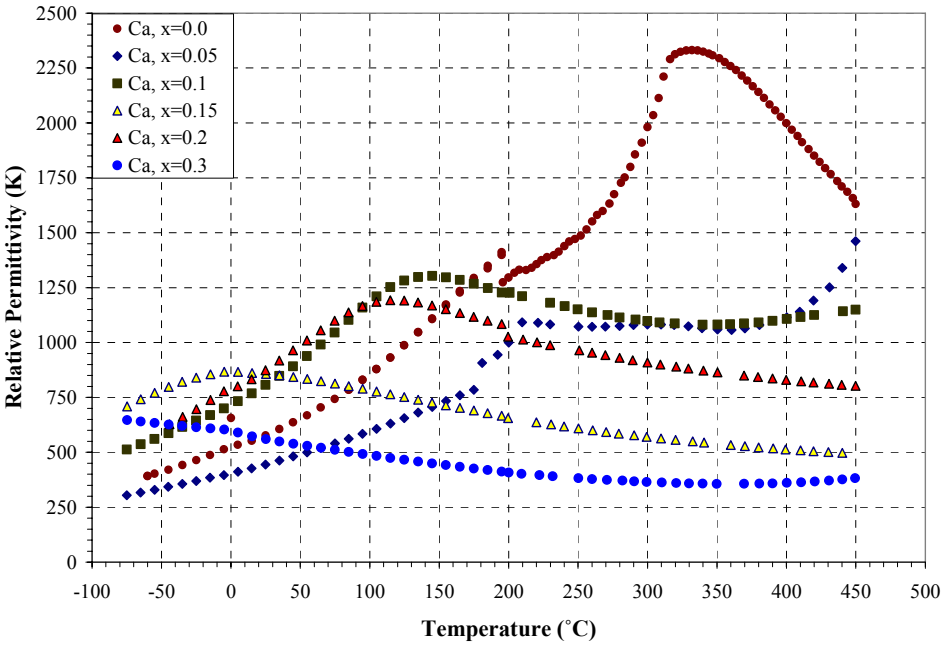

Figure 13. Relative permittivity at 10 kHz versus temperature for calcium doped BNT. Measurements were taken on cooling up to 200°C and on heating from 200°C to 450°C.

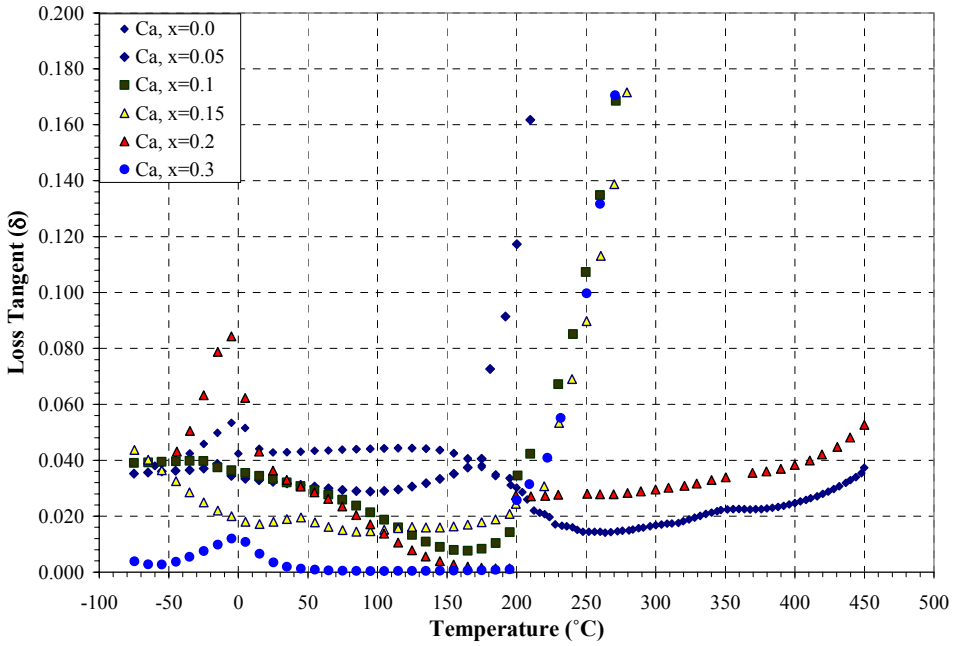

Figure 14. Loss tangent (δ) at 10 kHz versus temperature for calcium doped BNT. Measurements were taken on cooling up to 200°C and on heating from 200°C to 450°C.

4. $(Bi_{0.5} Na_{0.5}) [Sn_y Ti_{1-y}] O_3$

Tin (Sn^{4+}) was added to the structure according to the following stoichiometric formula, $(Bi_{0.3} Na_{0.3}) [Sn_y Ti_{1-y}] O_3$. It should be noted that Sn^{4+} is substituting for Ti^{4+} on the B-site of the structure. Tin additions to the B-site of BNT did not affect the peak temperature of the relative permittivity. As shown in Figure 15, the value of the peak relative permittivity was suppressed as the Sn level increased. The loss tangent (δ) for tin doped BNT is shown in Figure 16. Feng et al. found that Sn doping in lead zirconate titanate (PZT) also suppressed the peak value of the relative permittivity. They also noted that Sn stabilized the antiferroelectric phase of the PZT system.[35,36] The suppression of the peak is significant to the goal of this project because a flat dielectric response is necessary for the material to fit the requirements of an X7R material.

The peak relative permittivity is suppressed since tin is a larger cation than titanium and is therefore less polarizable. Tin is less polarizable because it is not a d^0 cation like titanium so there is no drive for hybrid or off center bonds to form. As more tin is added, the amount of polarizable titanium cations is reduced. The larger size of the

tin cation reduces the amount of displacement that can occur within the octahedral volume that is available. The reduction in the number of titanium cations is reflected in the peak suppression of the relative permittivity curves because tin has less space to displace in the octahedral cage.

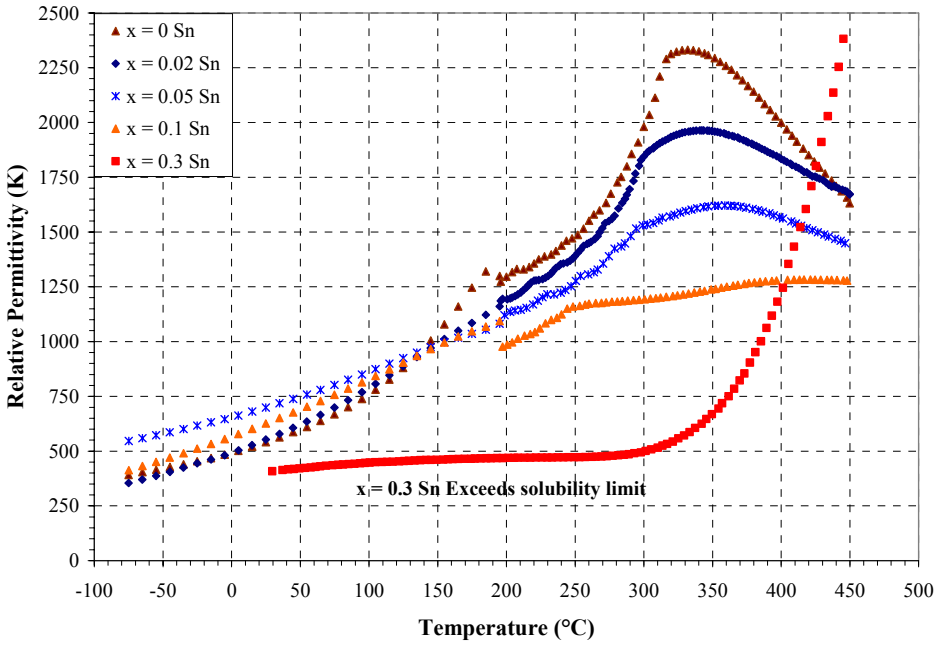

Figure 15. Relative permittivity at 10 kHz versus temperature for tin doped BNT. Measurements were taken on cooling up to 200°C and on heating from 200°C to 450°C.

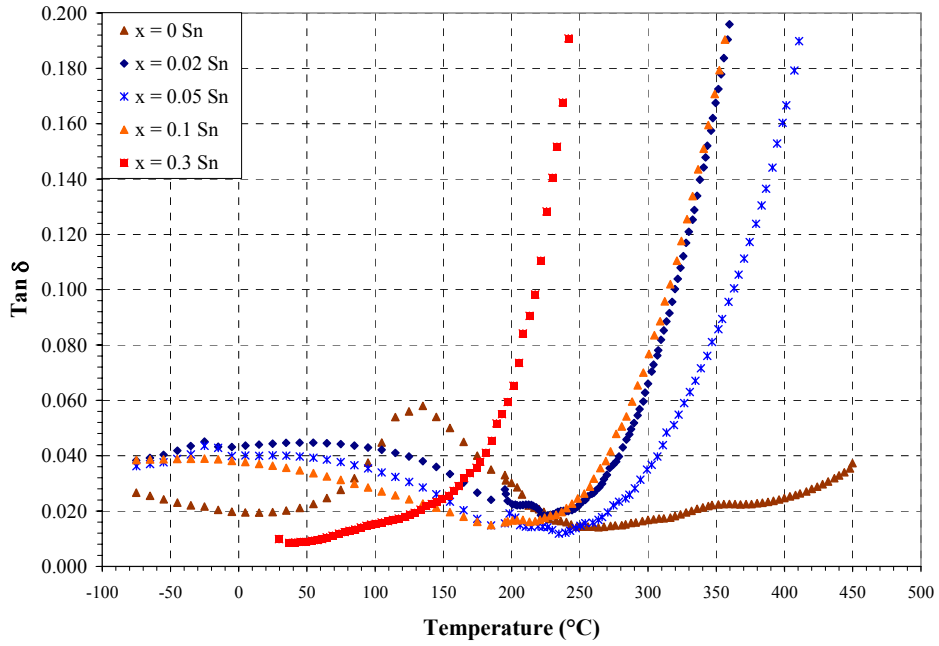

Figure 16. Loss tangent (δ) at 10 kHz versus temperature for tin doped BNT. Measurements were taken on cooling up to 200°C and on heating from 200°C to 450°C.

5. $(Bi_{0.5}Na_{0.5})[Zr_yTi_{1-y}]O_3$

Zirconium (Zr^{4+}) can be substituted for Ti^{4+} on the B-site in BNT by using the formula, $(Bi_{0.5}Na_{0.5})[Zr_yTi_{1-y}]O_3$. Figures 17 and 18 show the relative permittivity (K) and loss tangent (δ) versus temperature for compositions with y = 0.0, 0.02, 0.05, 0.1 and 0.2. As shown in Figure 17, the compositions where y = 0.02 and 0.05 enhance the 'shoulder' that is present at approximately 150°C. As the amount of Zr^{4+} increases beyond y = 0.05, the 'shoulder' disappears and the peak relative permittivity is suppressed and decreased to slightly lower temperatures. The behavior shown in the graph suggests that there is a small window where Zr^{4+} doping stabilizes the antiferroelectric phase that has been described in this region of BNT.[16,22,37] In lead zirconate titanate (PZT), the antiferroelectric phase can be stabilized by specific ratios of zirconium, titanium and tin.[35] In BNT, there may be a zirconium to titanium ratio that causes the antiferroelectric phase to be stabilized. Once the amount of zirconium exceeds the stabilization limit, it begins to suppress the peak relative permittivity just like the tin doped samples.

The peak suppression is similar to that seen in the tin doped samples discussed earlier. The mechanism that causes the peak suppression also may be the same. Zirconium has a larger ionic radius than titanium, 0.72 Å for Zr^{4+} versus 0.605 Å for 6 coordinate ions. The larger size leads to a decrease in polarizability of the ion because there is less room for the ion to displace within the octahedral cage. As the amount of zirconium increases, the amount of polarization contributed by the titanium ions decreases; therefore, the relative permittivity should also decrease, as seen in the graph.[10]

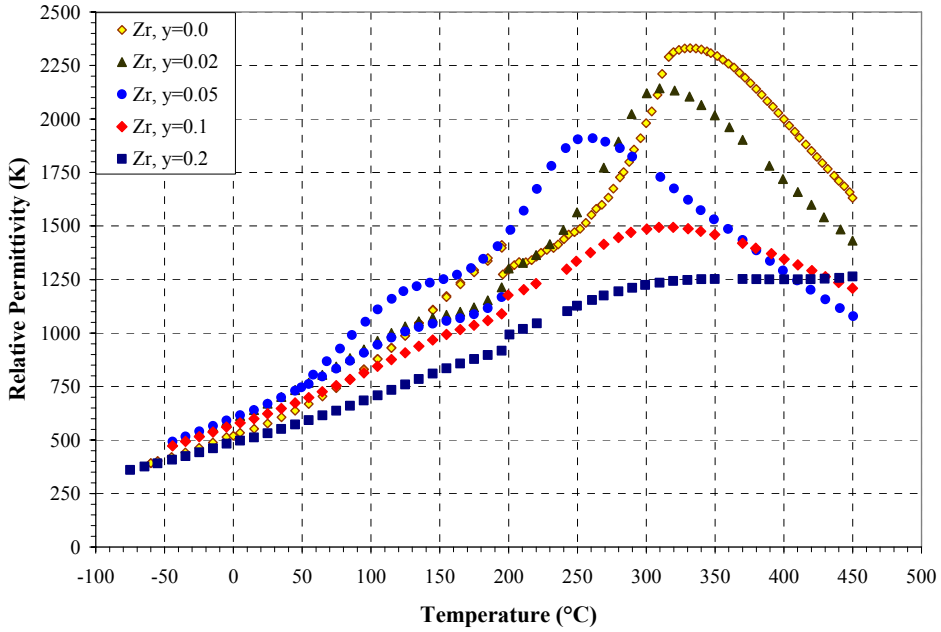

Figure 17. Relative permittivity at 10 kHz versus temperature for zirconium doped BNT. Measurements were taken on cooling up to 200°C and on heating from 200°C to 450°C.

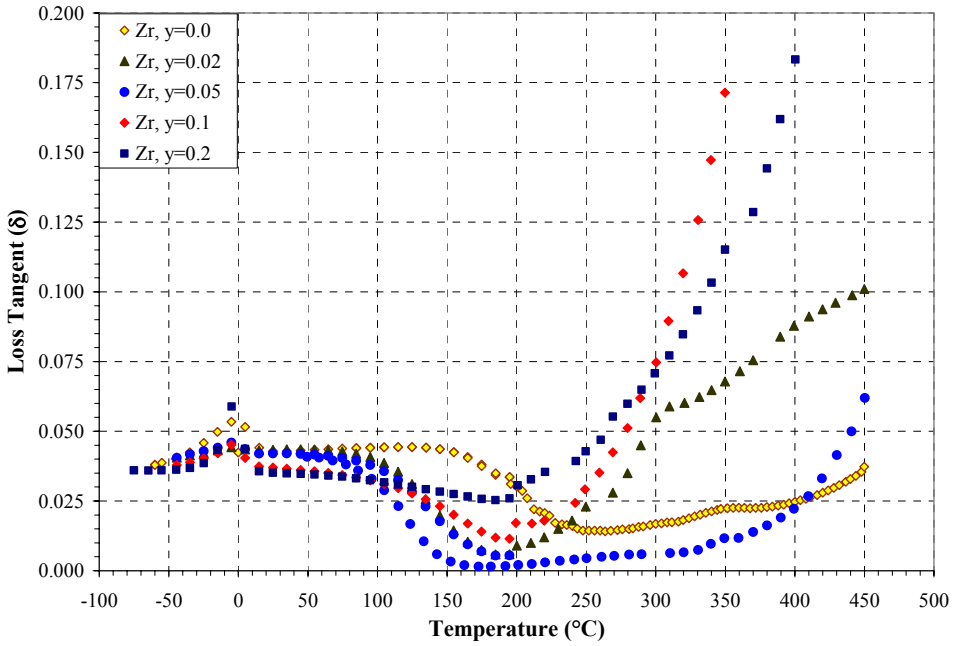

Figure 18. Loss tangent (δ) at 10 kHz versus temperature for zirconium doped BNT. Measurements were taken on cooling up to 200°C and on heating from 200°C to 450°C.

6. $[(Bi_{0.5}Na_{0.5})_{1-x}Ba_x][Sn_yTi_{1-y}]O_3$

Until now, the discussion has focused only on single dopants in BNT. Single dopants are useful for determining the behavior of the dopant in the material, however; they are insufficient to modify the structure to meet a specific goal. Multi-component systems, on the other hand are useful for modifying the structure to meet specific requirements. The behavior of two or more dopants can be combined to modify more than just the peak temperature or relative permittivity. They can modify multiple variables to create a material that is useful for many different applications.

One of the multi-component systems studied was BNT doped with barium (Ba^{2+}) on the A-site and tin (Sn^{4+}) for titanium on the B-site. They were combined at levels of x = y = 0.02, 0.05, 0.1, 0.2, according to the formula $[(Bi_{0.5}\ Na_{0.5})_{1-x}\ Ba_x]\ [Sn_y\ Ti_{1-}y]O_3$. Figures 19 and 20 show the relative permittivity and loss tangent (δ) versus temperature behavior of the formula mentioned above. The goal of multi-component systems is to take the individual properties of each dopant and try to create a material that displays those properties together.

According to the previous discussion, adding barium should increase the relative permittivity and decrease the peak temperature to 200°- 250°C, while increasing tin should suppress the peak relative permittivity. Figure 19 illustrates that the peak temperature decreases as the amount of barium is increased and that the peak becomes suppressed as the amount of tin is increased. The figure also shows that the relative permittivity starts out much larger than pure BNT at x = y = 0.02, 0.05 and 0.1. The permittivity does, however, decrease as the amount of barium and tin is increased. According to the results, all three characteristics that were present in the single component systems are still present in the multi-component system. This is because both barium and tin were added at the same level as described above. The suppression of the peak is caused by the decrease in polarizability as the amount of tin increases and the amount of titanium decreases.

The results of this system are promising because they show that multiple dopants can be added successfully to BNT to modify the structure. The fact that all of the characteristics are still present in the new system is promising for future systems because if different dopants combine in the same way, controlling the properties of the material will become very predictable.

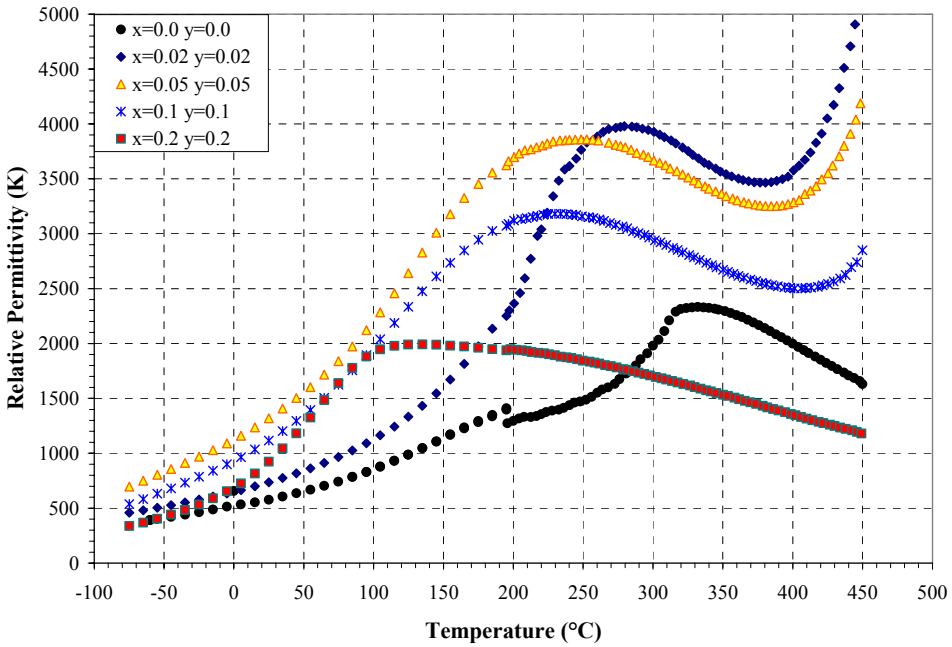

Figure 19. Relative permittivity at 10 kHz versus temperature for barium and strontium doped BNT. Measurements were taken on cooling up to 200°C and on heating from 200°C to 450°C.

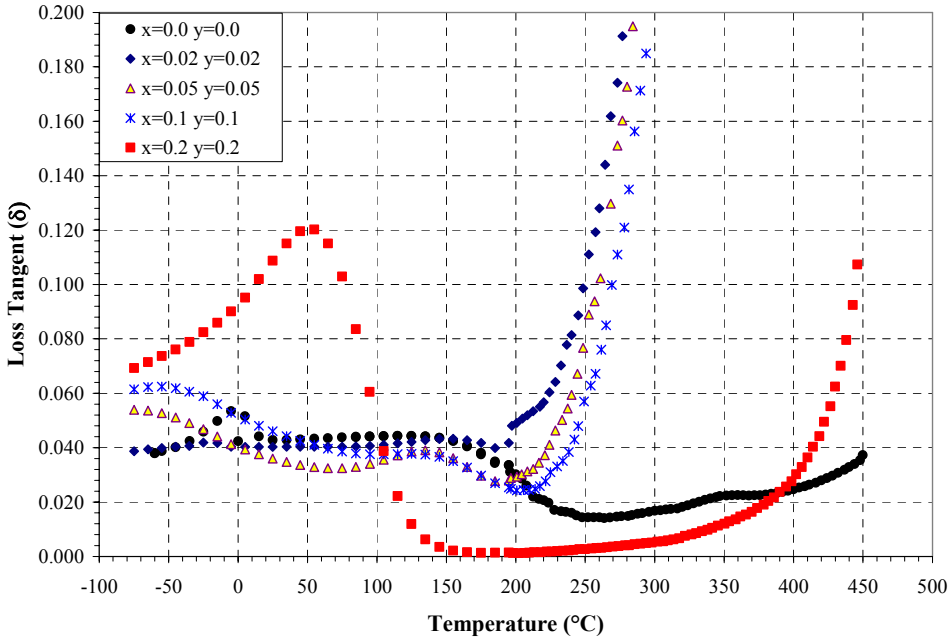

Figure 20. Loss tangent (δ) at 10 kHz versus temperature for barium and strontium doped BNT. Measurements were taken on cooling up to 200°C and on heating from 200°C to 450°C.

7. $[(Bi_{0.5}Na_{0.5})_{1-x-y}Ba_xSr_y][Sn_zTi_{1-z}]O_3$

Multi-component system doping has been determined to be useful for modifying the properties of BNT. Another system that was studied was a barium, strontium and tin doped BNT with x, y and z ranging from 0.0 to 0.3. Table II shows the compositions that were made for this study. Barium and strontium substitute for bismuth and sodium on the A-site of the structure because they are both 2+ cations, while tin substitutes for titanium on the B-site of the structure because it is a 4+ cation. The sintering schedule of this system had to be modified depending on the structure because barium and strontium are highly refractory materials. As the amount of barium and strontium was increased, the sintering time or temperature had to be changed to achieve a fully sintered pellet. The sintering temperatures and times are listed in Table II below for each composition.

This multi-component system was chosen because the low temperature (less than room temperature) relative permittivity of the Ba-Sn composition was lower than desired. Strontium was chosen as a third component because it decreases the peak temperature more effectively than barium. Strontium has similar characteristics to barium; however, barium only decreases the peak temperature to approximately 150°C, while the peak temperature for strontium additions decreases linearly as shown in Figure 12 to near absolute zero. The goal in this system was to expand on the previous results to try and increase the permittivity at the low end of the temperature range.

The relative permittivity (K) and loss tangent (δ) are shown in Figures 21 and 22. In order to create a relatively flat response tin was added at fairly high levels to each of the compositions. The peak suppression that is created by tin is useful because one of the goals is to maintain the relative permittivity within a ±15% range of the permittivity at room temperature. The relative permittivity values in Figure 21 are comparable to the permittivity value for the 20% Ba 20% Sn compound in Figure 19 above. Again, the low permittivity values are caused by the decreased polarizability that is created by the large amounts of tin in the structure. The results are promising for this structure because the strontium additions did help to decrease the peak temperature of relative permittivity to lower temperatures than the Ba-Sn compounds. As noted previously, the property trends for single dopants can be maintained in a multi-dopant system to more easily control the properties of the material.

Sample number 7 from the Table II, where (x = y = 0.3, z = 0.0) is an interesting sample because the peak temperature is low as expected; however, it exhibits a very high relative permittivity compared to the rest of the samples. This has to do not only with the lack of tin in the system, but with the tolerance factor that was discussed earlier. Sample number 7 is the only sample with a bond valence tolerance factor (Equation 5) greater than 1.0. As stated earlier, if a material has a tolerance factor greater than 1.0, the polarization in the material is expected to come from B-site distortions instead of the A-site. This composition is interesting because it has a permittivity larger than 1000 (K) over the temperature range of -60°C to 375°C. The loss tangent (δ) remains below 0.1 over the same temperature range. This sample is very interesting because it meets every goal accept the percent change of ±15 discussed above.

Overall, this multi-component system showed that the consolidation of properties of single dopants could be extended to a three-component system. Many more compositions could be made where the barium and strontium amounts are allowed to vary independently; however, that study is beyond the scope of this thesis. It is possible that a composition in this system could be found to comply with all of the requirements of the project if each of the dopants were varied independently to optimize the properties of the material.

Table II. This Table Shows the Compositions, Sintering Conditions and Geometrical Densities for the Barium-Strontium-Tin Multi-component System.

$[(Bi_{0.5}Na_{0.5})_{1-x-y}Ba_xSr_y][Sn_zTi_{1-z}]O_3$						
	Ba = x	**Sr = y**	**Sn = z**	**Temperature (°C)**	**Time (minutes)**	**Density (g/cm^3)**
1	0.05	0.05	0.15	1200	30	5.76
2	0.05	0.05	0.3	1200	30	5.74
3	0.15	0.15	0.15	1200	120	5.63
4	0.15	0.15	0.25	1200	120	5.69
5	0.2	0.2	0.1	1300	60	5.36
6	0.25	0.25	0.2	1300	60	5.46
7	0.3	0.3	0	1300	60	5.08

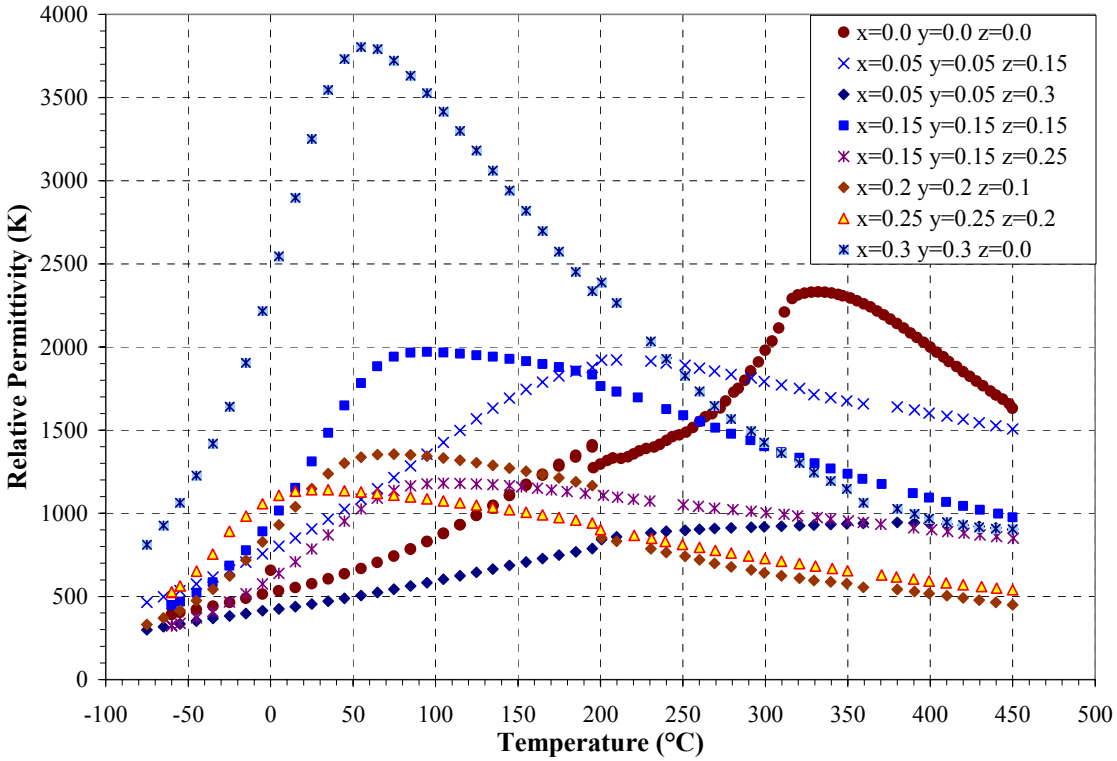

Figure 21. Relative permittivity at 10 kHz versus temperature for barium, strontium and tin doped BNT. Measurements were taken on cooling up to 200°C and on heating from 200°C to 450°C.

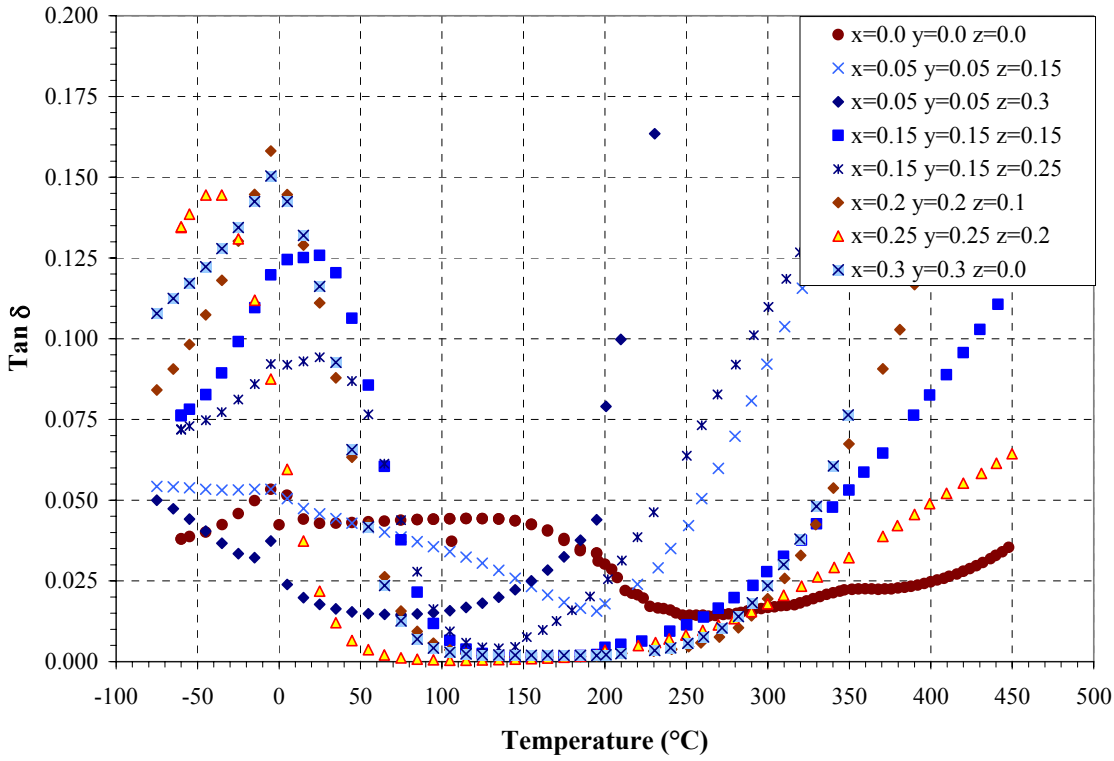

Figure 22. Loss tangent (δ) at 10 kHz versus temperature for barium, strontium and tin doped BNT. Measurements were taken on cooling up to 200°C and on heating from 200°C to 450°C.

8. $[(Bi_{0.5}\ Na_{0.5})_{1-x}\ Ba_x]\ [Zr_y\ Ti_{1-y}]O_3$

Another multi-component system that was studied was BNT doped with Ba^{2+} on the A-site for bismuth and sodium, and Zr^{4+} on the B-site for titanium. The relative permittivity and loss tangent are shown in Figures 23 and 24, respectively. The dopants were added according to the formula $[(Bi_{0.5}\ Na_{0.5})_{1-x}\ Ba_x]\ [Zr_y\ Ti_{1-y}]O_3$. Results by Sheets et al., led to an emphasis on a zirconium level of y=0.04. Sheets et al. determined that the 'shoulder' present near 100° to 150°C could be optimally enhanced by adding zirconium at the 4 mol % level.[15]

It has been shown that barium doped BNT has an MPB near 7 mol %. It has also been shown that adding small amounts of zirconium (up to ~ 5 mol%) will enhance the 'shoulder' of the curve. By combining barium and zirconium, a broad peak was created with a large relative permittivity when compared to pure BNT. The problem with this composition is that the permittivity drops off fairly fast below 100°C in these materials.

The high temperature permittivity results are very attractive because the K is fairly high (around 3000-4000) and very broad. It may be possible to expand on this family of materials to create a material that has properties somewhere in the middle with a moderate relative permittivity over the desired temperature range.

Most of the results for this family showed promising results. The sample with Ba = 0.25 and Zr = 0.3 did not exhibit results similar to the rest. The relative permittivity for this sample is very low and flat. This leads to two conclusions. One conclusion is that the dopant level is too high so the structure became unstable. The other is that the pellet was not fully sintered so the density is very low resulting in the poor data. The latter of the two conclusions is the most probable because from previous examples, the higher dopant levels including barium needed to be fired at higher temperatures and longer times. The high loss shown in Figure 24 strengthens the conclusion that the low density is the cause of the poor results.

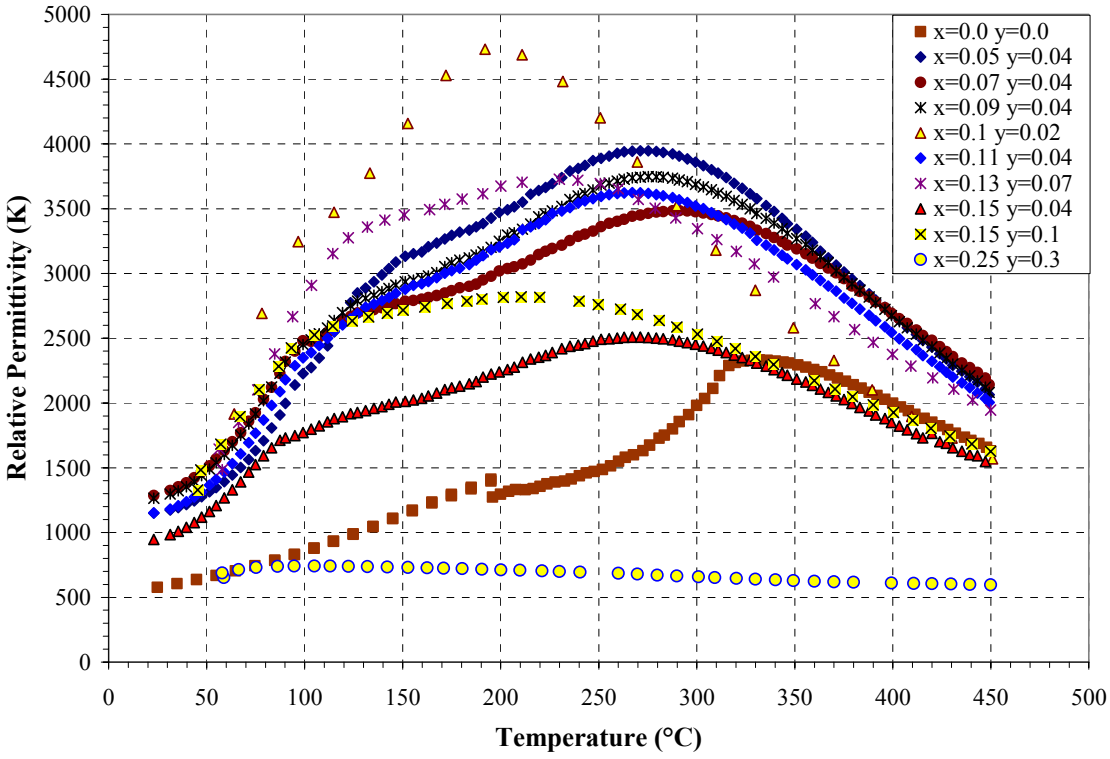

Figure 23. Relative permittivity at 10 kHz versus temperature for barium and zirconium doped BNT. Measurements were taken on heating from room temperature to 450°C.

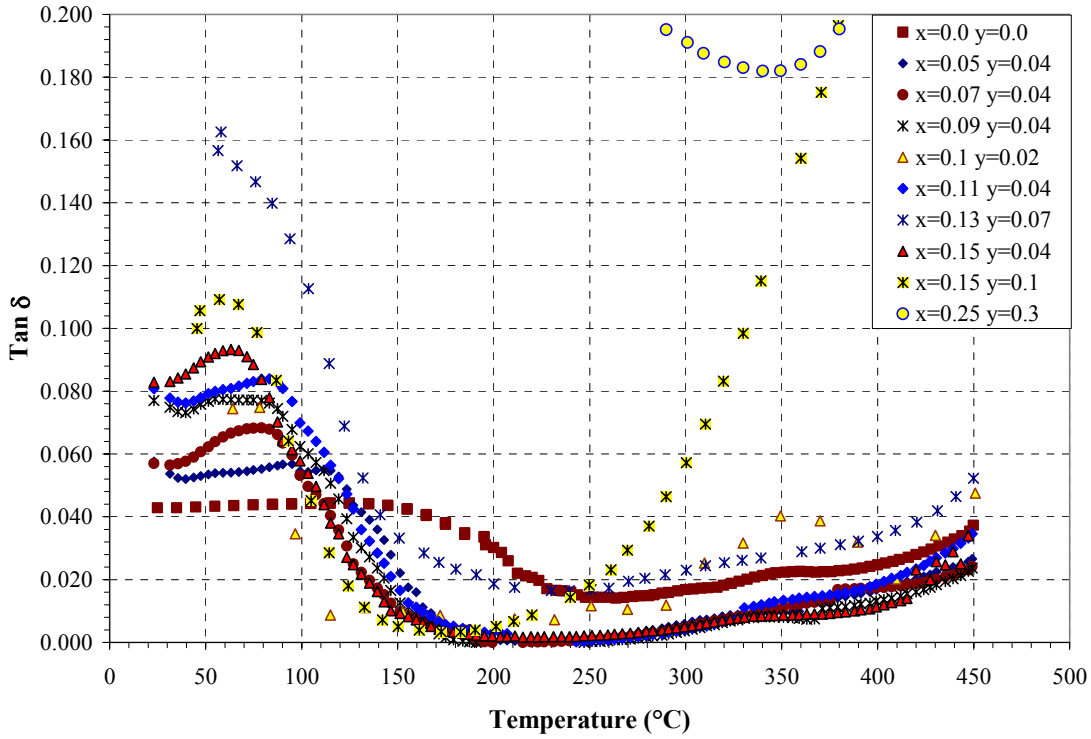

Figure 24. Loss tangent (δ) at 10 kHz versus temperature for barium and zirconium doped BNT. Measurements were taken on heating from room temperature to 450°C.

B. Rietveld Refinements

Rietveld refinements were performed on the strontium and tin doped BNT samples (results sections 2 & 4 above) and a sample of pure BNT powder. EXPGUI, a graphical user interface program for GSAS was used to perform the refinements because it is a powerful and user friendly interface.[55,56] The refinement results are tabulated in Table III below. The lattice parameters from this table were used in Figures 32 and 33.

Table III. Refinement Results Obtained for the Sr^{2+} and Sn^{4+} Doped Samples.

Formula	Crystal Structure	X^2	wRp	a (Å)	c (Å)
$(Bi_{0.5}\ Na_{0.5})\ TiO_3$	Rhombohedral	0.923(6)	0.116(6)	5.4802(7)	13.487(1)
$[Bi_{0.5}\ Na_{0.5})_{0.9}\ Sr_{0.1}]\ TiO_3$	Rhombohedral	1.09(1)	0.119(1)	5.4943(2)	13.5047(6)
$[Bi_{0.5}\ Na_{0.5})_{0.7}\ Sr_{0.3}]\ TiO_3$	Tetragonal	1.12(7)	0.122(7)	5.5154(1)	3.9225(2)
$[Bi_{0.5}\ Na_{0.5})_{0.5}\ Sr_{0.5}]\ TiO_3$	Tetragonal	1.14(4)	0.124(4)	5.5245(2)	3.9080(4)
$(Bi_{0.5}\ Na_{0.5})\ [Sn_{0.02}\ Ti_{0.98}]O_3$	Rhombohedral	0.555(1)	0.092(1)	5.48722(7)	13.4926(3)
$(Bi_{0.5}\ Na_{0.5})\ [Sn_{0.05}\ Ti_{0.95}]O_3$	Rhombohedral	0.717(1)	0.098(1)	5.5018(1)	13.4485(7)
$(Bi_{0.5}\ Na_{0.5})\ [Sn_{0.1}\ Ti_{0.9}]O_3$	Rhombohedral	0.794(3)	0.104(3)	5.5033(1)	13.4591(5)

The X^2 value is the "goodness of fit" parameter for the refinements. It is a measure of the observed data versus the calculated data. A value of 1.0 represents a perfect fit for the refined structure. Chi squared values less than 1.0 represent results that have been fit with too many parameters for the quality of the gathered data. If the quality of the data is low, only a few parameters can be correctly refined. As the quality of the data increases, the number of parameters that can be refined also increases. X^2 values greater than 1.0 represent results that have been fit as well as possible; however, more parameters could be refined if the data were good enough to handle them. The wRp value is the residual error in the calculations and should be near 0.1 for a good fit.[57]

The refinements yielded lattice parameters and some ion position information for the structures. The ion positions are not refined very well, e.g. many of the ions are too small to refine using x-ray diffraction. The lattice parameter results were used as experimental values to compare with the theoretical values from the bond valence model. For example, if the ionic positions could be refined more exactly by using neutron diffraction, they could be imported into a program such as Powdercell to display the structure graphically. Powdercell is a program that uses the crystal structure information along with lattice parameters and ionic positions to plot the structure in three dimensions. These three dimensional pictures are very useful to help demonstrate the dopant effects in a visual way, rather than just the values determined by the Rietveld refinements. Powdercell calculates the bond lengths from the ion positions, which can be compared the structural model determined by the bond valence method.

Figure 25 shows a plot of pure BNT powder that was refined using the Rietveld method. The refinement was performed at room temperature under the conditions described in the experimental procedure section. The structure refined fairly easily by using the initial data from the crystallographic information file created by Jones and Thomas.[4] The slight mismatch in the amplitude seen in the peak at approximately 47° 2-theta for the BNT sample likely reflects the poor refinement precision for the x-ray data.

Figures 26-28 show plots of the Rietveld refinements for the x = 0.1, 0.3 and 0.5 Sr samples respectively. Figures 29-31 show plots of the Rietveld refinements for the y = 0.02, 0.05, and 0.1 Sn samples respectively. The plots show the observed, calculated and

observed minus calculated curves, which graphically reflect the goodness of fit. They can offer easily understood indicators of a poor parameter fit.

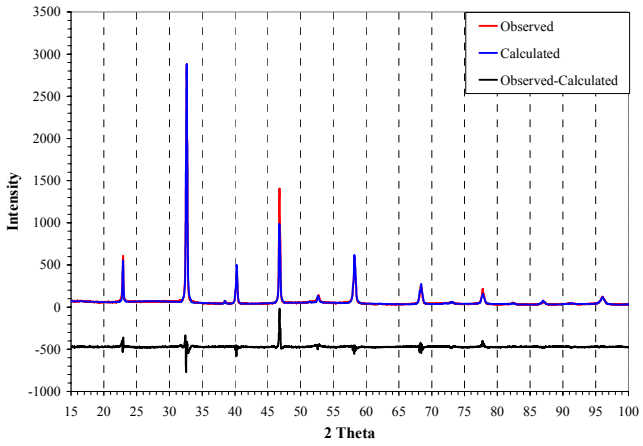

Figure 25. Rietveld refinement plot (rhombohedral) showing the observed, calculated and observed minus calculated curves for 100% BNT. (Note: Observed and calculated curves are overlapping.)

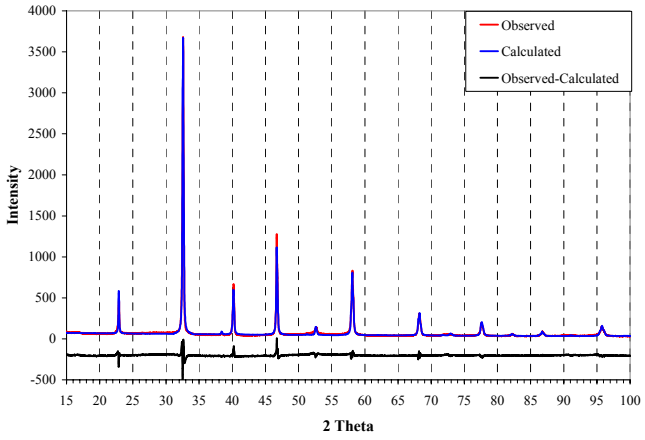

Figure 26. Rietveld refinement plot (rhombohedral) showing the observed, calculated and observed-calculated curves for Sr = 0.1 doped BNT. (Note: Observed and calculated curves are overlapping.)

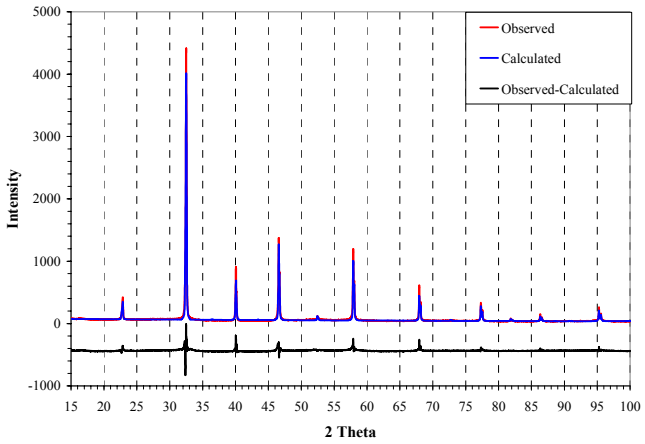

Figure 27. Rietveld refinement plot (tetragonal) showing the observed, calculated and observed-calculated curves for Sr = 0.3 doped BNT. (Note: Observed and calculated curves are overlapping.)

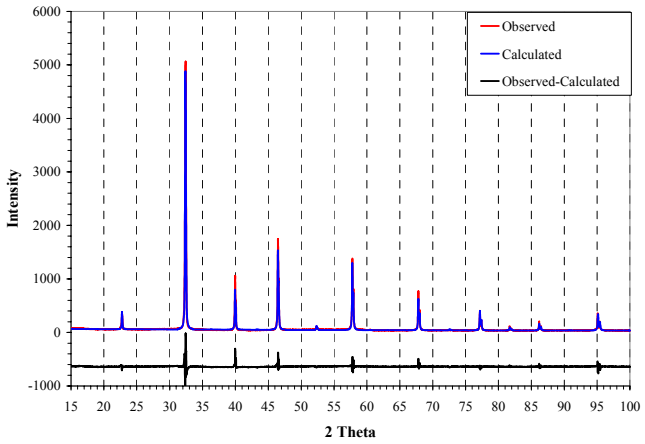

Figure 28. Rietveld refinement plot (tetragonal) showing the observed, calculated and observed-calculated curves for Sr = 0.5 doped BNT. (Note: Observed and calculated curves are overlapping.)

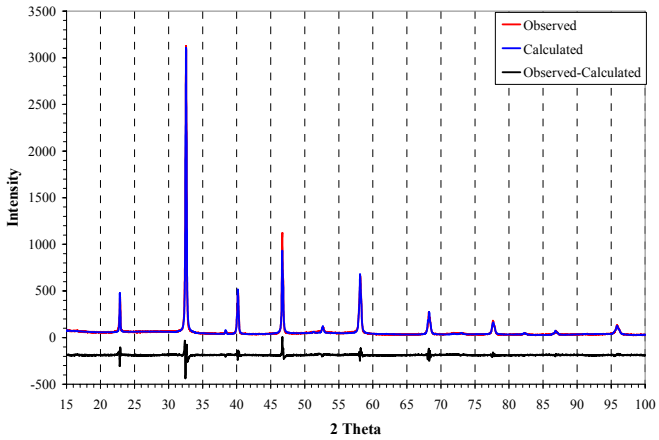

Figure 29. Rietveld refinement plot (rhombohedral) showing the observed, calculated and observed-calculated curves for Sn = 0.02 doped BNT. (Note: Observed and calculated curves are overlapping.)

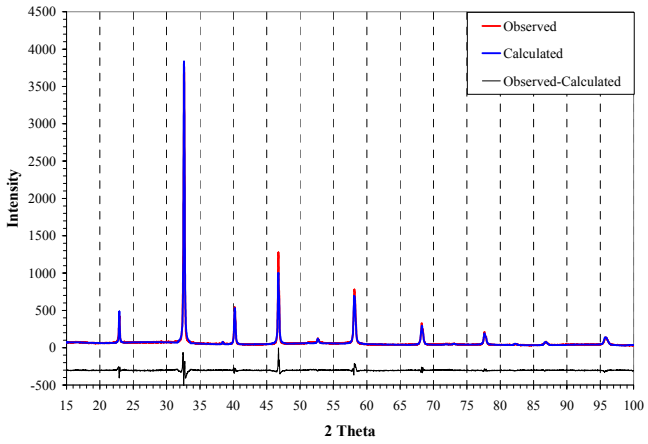

Figure 30. Rietveld refinement plot (rhombohedral) showing the observed, calculated and observed-calculated curves for Sn = 0.05 doped BNT. (Note: Observed and calculated curves are overlapping.)

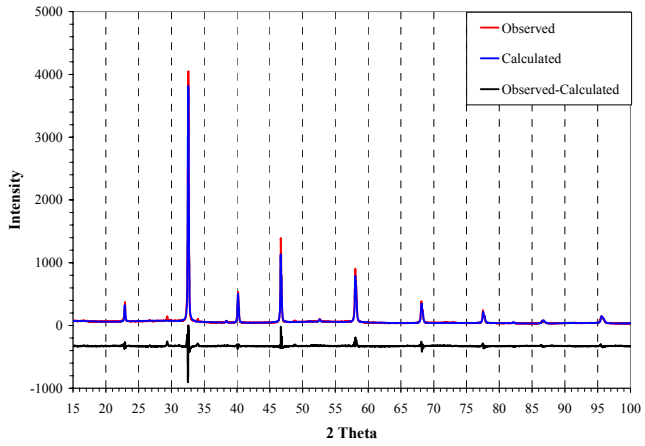

Figure 31. Rietveld refinement plot (rhombohedral) showing the observed, calculated and observed-calculated curves for Sn = 0.1 doped BNT. (Note: Observed and calculated curves are overlapping.)

C. Bond Valence Analysis

The bond valence method was utilized for this project by creating tolerance factor charts that indicate how a particular dopant affects the stability of BNT. The charts also usefully compare the various dopant effects to each other. Figures 32 and 33 show the effects of A and B-site dopants respectively on the bond valence tolerance factor of BNT.

When there is a mismatch between the lattice parameters calculated from the A-O bonds and the B-O bonds, the lattice must strain to allow the structure to form. The tolerance factor is a measure of the amount of mismatch between the bonds. Equation 8 below is used to convert the bond lengths for the structure into lattice parameters. When the A and B-site bonds require different lattice parameters, as is the case for BNT, some bonds lengthen while others shorten to allow the structure to form. The lengthening of some bonds and shortening of others creates the lattice strain in the material. According to the bond valence model, the structure will always distort around the bonds that are in tension.[38,58-62]

In BNT, the A-site cations require lattice parameters that are smaller than the B-site cations. According to the tolerance factor equation, that ratio causes the tolerance factor to be less than 1.0. Dopants that cause the tolerance factor to decrease in BNT cause the lattice strain to increase because they are increasing the mismatch between the A and B-site lattice parameters. Dopants that cause the tolerance factor to increase on the

other hand, cause the lattice strain to decrease because they are decreasing the mismatch between the A and B-site lattice parameters.

As the charts show, some dopants cause the tolerance factor to increase, while others cause the tolerance factor to decrease. The A-site dopants that cause an increase in tolerance factor tend to cause the structure to transition into the tetragonal phase at lower temperatures. The phase transition is able to occur at lower temperatures because the lattice strain is reduced as the tolerance factor approaches 1.0. The strain is reduced because dopants with a positive tolerance factor slope decrease the mismatch between the A and B-site lattice parameters. On the other hand, dopants that decrease the tolerance factor tend to stabilize the rhombohedral phase to higher temperatures for the opposite reason. Dopants with a negative slope increase the lattice strain because they are increasing the lattice parameter mismatch between the A and B-site.

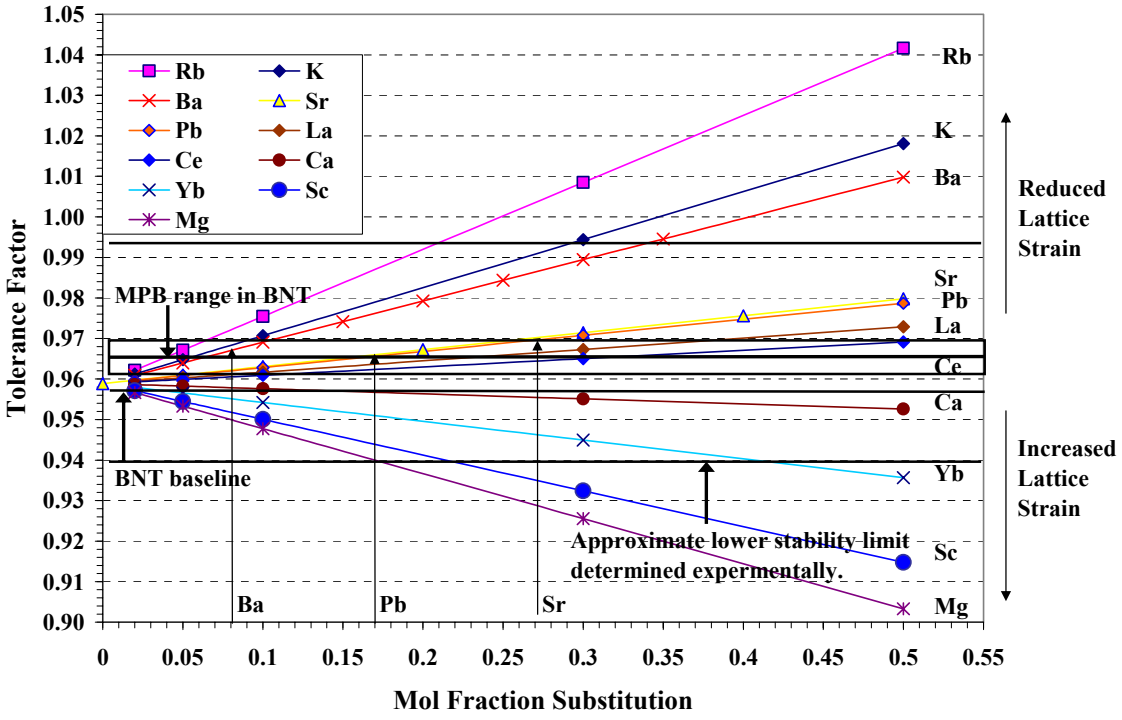

Figure 32. The affects of 12 coordinate A-site dopants on the bond valence tolerance factor for bismuth sodium titanate. The Ba, Pb, and Sr arrows show the respective amounts necessary to form an MPB composition.

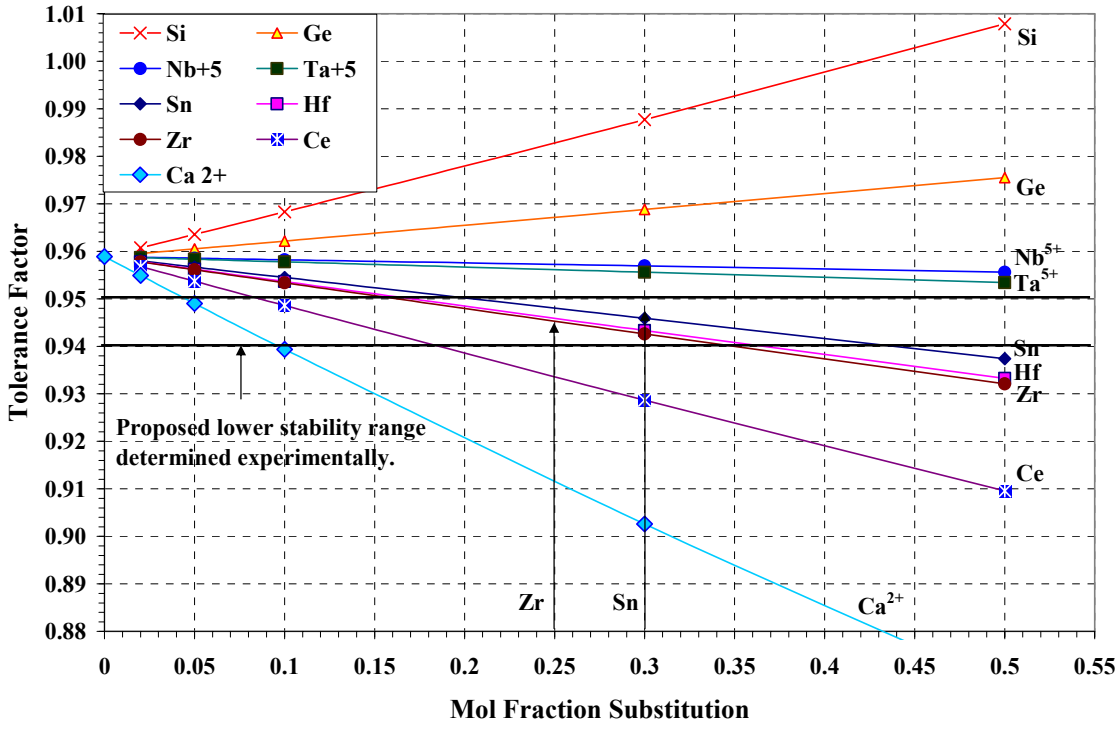

Figure 33. The affects of 6 coordinate B-site dopants on the bond valence tolerance factor for bismuth sodium titanate. The Zr and Sn arrows show their respective experimentally determined stability limit.

BNT samples doped with strontium and tin were measured by x-ray diffraction to compare the measured and calculated lattice parameters of the structure. The lattice parameters measured by x-ray diffraction were determined via Rietveld refinements. The results are shown in Figures 34 and 35 below. The results of the bond valence tolerance factor for A and B-site substituted BNT are shown in Figures 32 and 33 above. Figure 32 shows that as the strontium level is increased, the tolerance factor of the compound increases toward the undistorted value of 1.0. The increasing value suggests that strontium reduces the amount of octahedral distortion in the structure because it is alleviating the lattice parameter mismatch between the A and B-site. Figure 34 shows that both the measured and calculated lattice parameters for strontium doped BNT increase as the amount of strontium is increased. According to the tolerance factor equation, if the lattice parameter for the A-site is increased in BNT, the tolerance factor will approach 1.0.

As the amount of Sn increases on the B-site, the tolerance factor decreases farther away from the value of 1.0. According to the dielectric data, as the amount of tin increases, the peak of the dielectric constant becomes suppressed. This may be due to the fact that the tin is creating more distortion in the structure by increasing the mismatch between the A and B-site. The distortion is increased because the bond lengths predicted by the bond valence method for Ti-O bonds and Sn-O bonds are 1.965Å and 2.055Å respectively. These bond lengths can be converted into lattice parameters by using Equation 8 below. As discussed earlier, for tin cations to reside on the B-site of the perovskite structure, the lattice must increase in size, the Sn-O bonds must buckle, or a combination of both must occur. As the amount of tin is increased, the bond lengths increase; this increases the desired lattice parameter of the structure. The increase in desired lattice parameter creates a larger mismatch between the A and B-site. The larger mismatch causes the lattice strain to increase as discussed above. Figure 35 below shows that the calculated and experimental lattice parameters increase as the amount of tin increases.

The lattice parameters for the theoretical structures can be calculated by using Equation 8.[47]

$$a = 2^{1/2} R_{AO} = 2R_{BO} \tag{8}$$

Where: R_{AO} is the length of an A-O bond

R_{BO} is the length of a B-O bond

Equation 8 is useful for determining the theoretical lattice parameters for BNT structures that have been modified by a dopant. This is done by calculating the weighted average of the bond lengths of Na-O, Bi-O, Ti-O and dopant-O bonds on the A-site. The lattice parameters must also take the B-site cation into consideration because the ideal overall cell model is an average of the A and B-site bond lengths. Any mismatch in the lattice parameters calculated by the A-O bonds and B-O bonds must be alleviated by a distortion in the system.[38]

The theoretical lattice parameters are based on a cubic lattice structure with a Pm3m space group. This is different from the R3c rhombohedral space group, which is based on hexagonal axes. The tetragonal P4bm space group is also not a primitive cell. The lattice parameters for the pseudocubic structure within the R3c space group can be

obtained by plotting the structure in Powdercell using the information from the refined structure. From there the A-site to A-site bonds can be displayed describes the (a) lattice parameter of the pseudocubic cell. A factor of $2^{1/2}$ can be used to change between the pseudocubic and the rhombohedral or tetragonal lattice parameters. These lattice parameters are compared to the calculated values to determine the accuracy of the model. Figures 34 and 35 show the theoretical lattice parameters for the Sr and Sn structures calculated via the weighted averages of Equation 8, and the experimental values determined by the Rietveld refinements. The lattice parameters measured for the strontium doped samples are rhombohedral R3c for the Sr = 0.1 and tetragonal P4bm for the Sr = 0.3 and 0.5. For the tin doped samples, all of the lattice parameters measured are for rhombohedral R3c structure.

The lattice parameter values of the calculated and measured are within a few hundredths of an Angstrom for both the strontium and tin doped the samples. As the graphs show, the theoretical values are less than the experimental values; this result could be expected because the experimental structure would generally not fit together as exactly as the theory predicts. There are also distortion issues discussed above that are not easily modeled by the theoretical values. Modifications must be made to the theoretical calculations to more accurately describe the experimental values and to more fully understand why the differences exist. Neutron diffraction data could be used to modify the model because the ion positions for the structure would then be known.

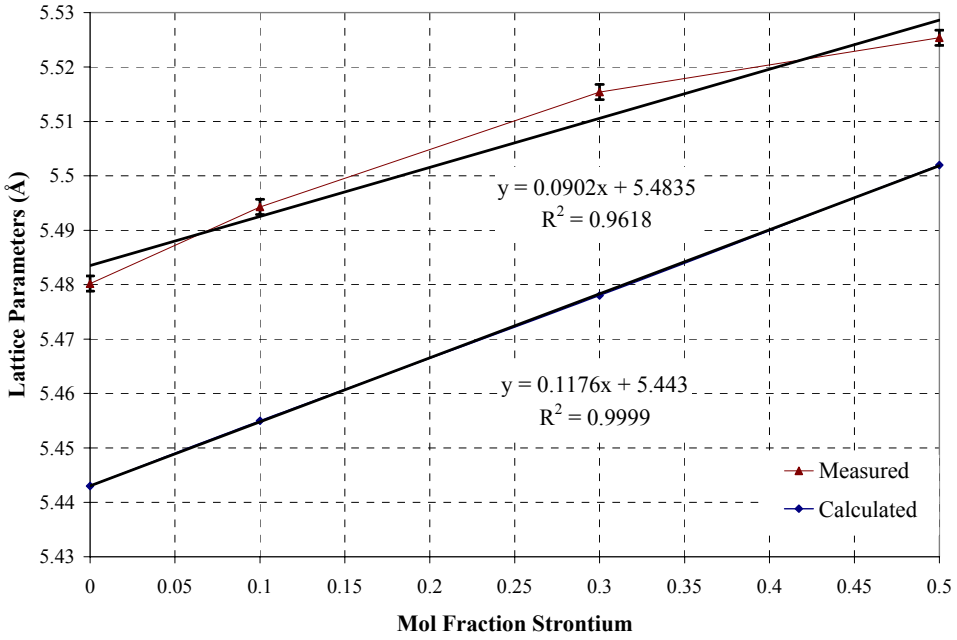

Figure 34. Measured and calculated lattice parameters for strontium doped BNT. The error bars indicate 2 times the largest error (from Table III) for the refinement and the trend line indicates the linear fit between the calculated and measured lattice parameters.

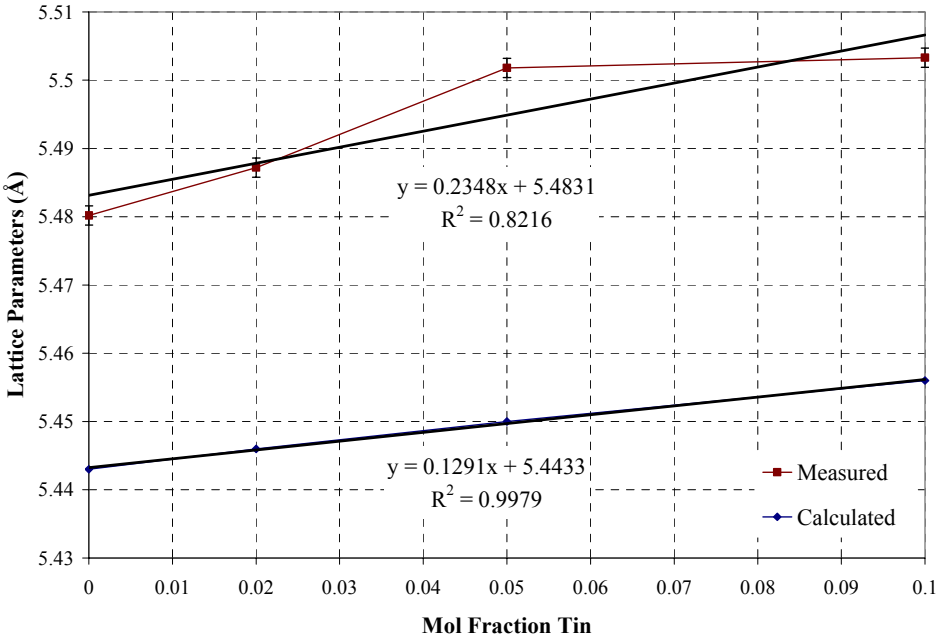

Figure 35. Measured and calculated lattice parameters for tin doped BNT. The error bars indicate 2 times the largest error (from Table III) for the refinement and the trend line indicates the linear fit between the calculated and measured lattice parameters.

1. Bond Valence Results: Barium and Strontium doped BNT.

Barium and strontium both have increasing tolerance factor values in BNT. Barium and strontium both decrease the internal structural strain because they are replacing smaller cations. By replacing small cations with larger cations, the A-site bonds are not stretched as much. The lattice parameters for barium and strontium doped BNT are predicted to increase. The predicted increase in lattice parameters is a result of the R_0 value for both Ba and Sr being larger than the average R_0 value of Bi and Na. As discussed earlier, the rhombohedral phase of BNT has $a^-a^-a^-$ octahedral tilting. The tetragonal phase has $a^0a^0a^-$ octahedral tilt. Both barium and strontium additions cause the octahedral tilt to decrease in the rhombohedral phase, along with the decrease in lattice strain. The decrease in octahedral tilt allows the structure to transform to the tetragonal phase at lower temperatures because the bonds do not have to expand as much before the phase will change. The decrease in octahedral tilt angle and the increase in lattice parameters with the addition of barium both contribute to the decrease in phase transition temperature from rhombohedral to tetragonal.

2. Bond Valence Results: Calcium doped BNT.

Calcium doped BNT is an interesting system that shows promising dielectric properties at temperatures below 0° C. Calcium is considered an A-site dopant that replaces both bismuth and sodium, however in some cases calcium has been found to go into the structure in small amounts on the B-site. The batch formulations for this system were set up in a stoichiometric way as to promote only A-site doping. The amount of bismuth and sodium was reduced by the same amount of calcium that was to be added. Even though these precautions were taken, there is no way to be sure that some cations did not go to the B-site to replace titanium cations.

According to Figures 32 and 33, calcium has little affect on the A-site tolerance factor, however it has a large affect on the B-site tolerance factor. If in fact some small amount of calcium cations, maybe 1 to 5 mol % can substitute for titanium on the B-site, the effects of both A and B-site tolerance factor must be examined. The best low temperature dielectric properties were exhibited by the 15 mol % calcium doped BNT samples. This addition level could be yielding the best properties because it may be a combination of A and B-site doping. Calcium has a drastic affect on the B-site tolerance

factor because it is such a large cation compared to titanium. The drastic drop in tolerance factor supports the argument that only a small amount of calcium can substitute on the B-site. If more than approximately 5 mol % calcium substitutes on the B-site, the structure should no longer be stable according to the trends that have been seen from other B-site dopants.

3. Bond Valence Results: Tin and Zirconium doped BNT.

Tin and zirconium both have a negative slope on the B-site tolerance factor chart in Figure 33. The negative slope on the B-site tolerance factor chart says that the cations are larger because for the tolerance factor to decrease with B-site additions, the B-O bond length must increase. The increase in bond length is caused by an increase in the average B-site cation size. The R_0 values for tin and zirconium are larger than the Ti value. According to the bond valence equation, and increase in R_0 will cause the calculated bond lengths to increase. When the B-site bond lengths increase, the lattice parameters of the structure should increase. If the lattice parameters would prefer a lattice parameter increase but are restricted by the A-site, the lattice strain will increase. When the distortion and strain increase, the rhombohedral structure is stabilized to higher temperatures. If the lattice strain increases too much, the structure will no longer be stable and the dielectric properties will be depleted.

4. Bond Valence Results: Barium-Tin Co-doped BNT.

Barium and tin individually have different slopes in their respective tolerance factor charts. Both of the dopants however have the same affect on the lattice parameters in that they cause the lattice parameters of the structure to increase. The chart in Figure 36 shows the bond valence tolerance factor with barium and tin additions to BNT. In this type of tolerance factor chart, one of the dopants is plotted along the x-axis, while the other dopants increase as the lines increase from bottom to top. For the purpose of uniformity, the B-site dopants have been plotted along the x-axis for each of the co-doped tolerance factor charts. The circles on the chart denote the compositions that were made for relative permittivity measurements.

These charts are used to select an array of compositions that covers a wide range in the tolerance factor. Four compositions were chosen for this system to test the

usefulness of these charts in determining the behavior of the dielectric results. The increasing trend in the compositions chosen suggests that the tetragonal phase will be stabilized to lower temperatures because the tolerance factor is increasing. The dielectric properties support this trend because the phase transition temperature decreases as the amount of barium and tin is increased. The phase transition, however, is mainly controlled by the amount of barium because barium is the driving force behind the tolerance factor increase. The dielectric properties also show peak suppression as the amount of tin is increased. The peak suppression is caused by the replacement of titanium cations by tin cations which have a lower polarizability; therefore, causing a decrease in peak dielectric constant.

The bond valence tolerance factor charts are a useful way of comparing the affect that multiple dopants will have on the tolerance factor of BNT. They give a visual array of tolerance factors over a broad range of compositions. Simply using the A-site and B-site tolerance factor charts individually does not give a very good picture as to how different levels of dopants will modify the tolerance factor.

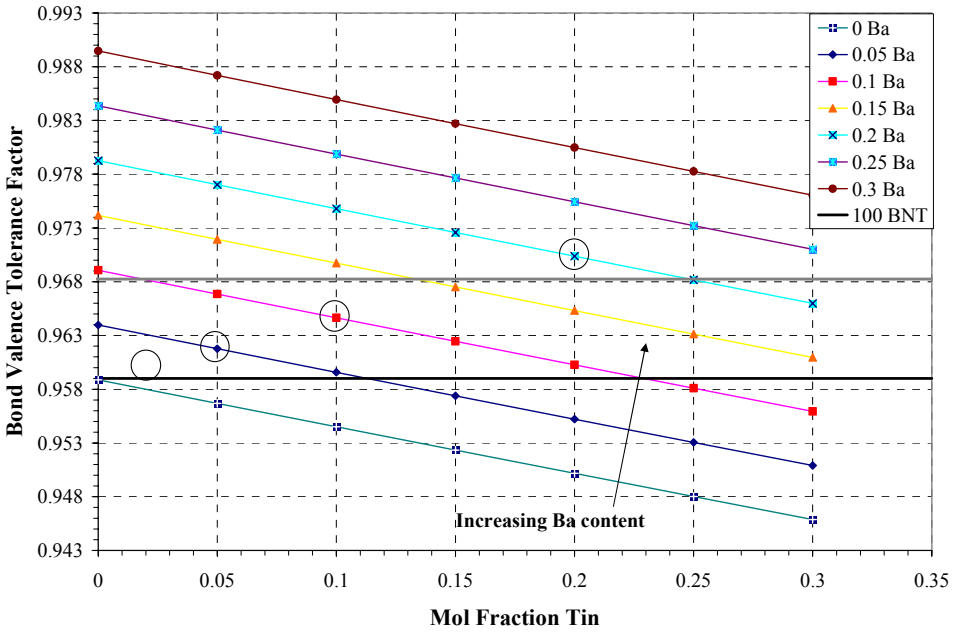

Figure 36. Bond valence tolerance factor chart for barium and tin co-doped BNT. (Y-intercept points are from Ba line of Figure 32).

5. Bond Valence Results: Barium-Strontium-Tin Co-doped BNT.

The barium-strontium-tin co-doped BNT samples cause the lattice parameters of the structure to increase because each of the cations is larger than the cations that they are replacing. Figure 37 was used to choose an array of compositions to test the dielectric properties of. They were chosen to try and cover each general area of the chart.

One of the compositions on the chart exceeded the 1.0 value. This composition was chosen to see if a noticeable difference could be seen in the properties. According to the dielectric properties, the composition of 30 mol % barium and 30 mol % strontium exhibited a greatly enhanced relative permittivity than the rest of the compositions. This was a promising result because when the tolerance factor is larger than 1.0, the polarization should come from the titanium cation moving out of the center of its octahedral cage. This is possible because the barium and strontium cations expand the A-site so much so that the A-site bonds are no longer in tension. When the tolerance factor is larger than 1.0, the B-site bonds become stretched so the titanium cation moves to a position out of the center of the octahedra to minimize the energy of the system. When the titanium cation moves out of center, a large polarization can occur depending on the magnitude of the displacement. As the relative permittivity results show for this system, the polarization of this composition is much larger than the compositions that were still distorted on the A-site of the structure.

The results discovered for this system of compositions are promising because they prove that the tolerance factor values can accurately describe the type of distortion that occurs in the structure. If a specific type of distortion or behavior is desired, the chart can be used to choose a small matrix of compositions around a specific tolerance factor to be tested. From that matrix, the best composition can be chosen for the job. With further study, the tolerance factor charts can be compared to the dielectric properties and other properties of the structure to determine ranges of similar behaviors, similar to a phase diagram. The goal is to reduce the number of compositions that needs to be made and measured to obtain an accurate description of the behavior of the system.

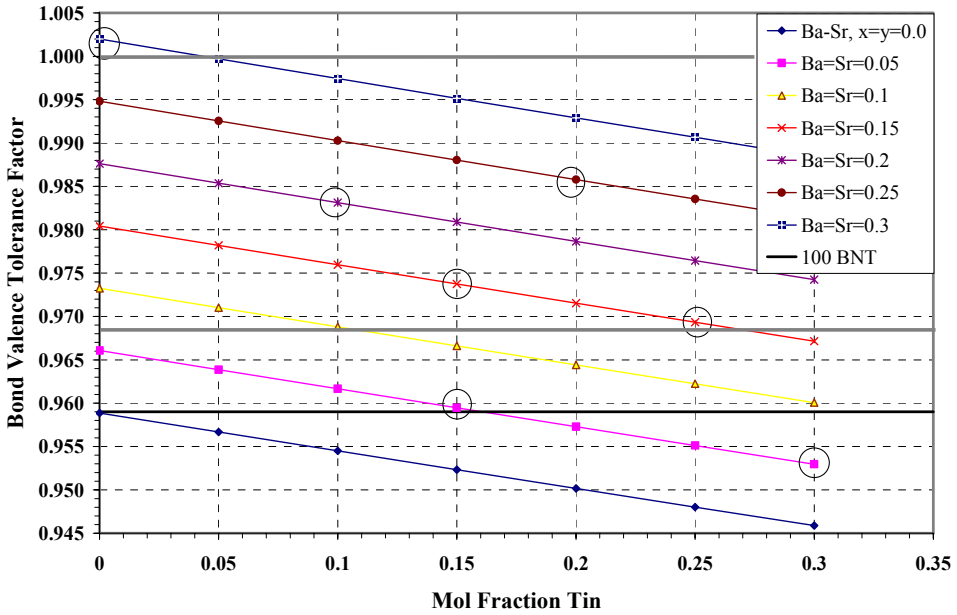

Figure 37. Bond valence tolerance factor chart for barium, strontium and tin co-doped BNT. (Y-intercept points are a combination of the Ba and Sr lines from Figure 32).

6. Bond Valence Results: Barium-Zirconium Co-doped BNT.

Barium and zirconium co-doped BNT combine the properties of both of the components. The bond valence analysis says that the lattice parameter will increase as the amount of barium and zirconium is increased because they are replacing smaller cations in the structure. Figure 38 shows the bond valence tolerance factor for the barium-zirconium co-doped BNT system. The compositions were chosen to utilize the morphotropic phase boundary behavior of barium and the shoulder enhancement of zirconium. The compositions that were chosen are denoted by the circles on the chart. As shown earlier, barium exhibits an MPB in BNT near the value of 0.968 ±0.005. Many compositions were chosen near this value and the relative permittivity for these compositions is very high as is expected for MPB compositions.

There is a limit, however, to the amount of zirconium that can be added to the structure before it becomes unstable and depletes the relative permittivity. The compositions with zirconium levels of 10 mol % and above begin to show the effects of the permittivity depletion. Unlike zirconium doped BNT a higher level of zirconium can be added to this system because the barium cations are expanding the A-site

simultaneously so that the lattice parameter mismatch does not become as severe as it could. The relative permittivity of the structure gets depleted because the zirconium cations are larger than the titanium cations, and therefore produce less polarization in the structure. Barium additions expand the A-site so that at low levels, zirconium additions do not diminish the relative permittivity as fast as they normally would.

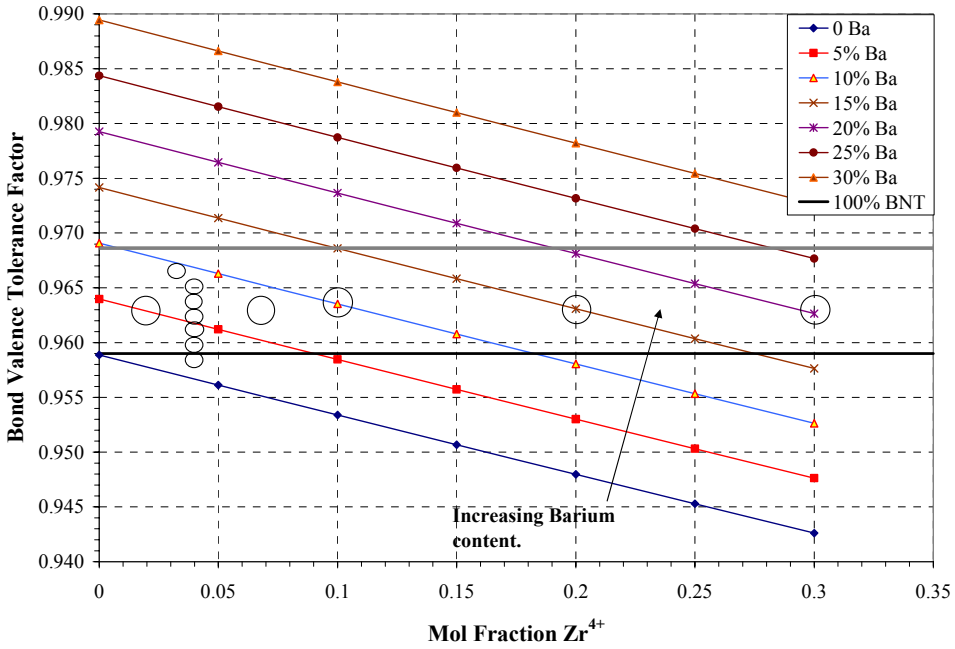

Figure 38. Bond valence tolerance factor chart for barium and zirconium co-doped BNT. (Y-intercept points are from Ba line of Figure 32).

IV SUMMARY AND CONCLUSIONS

An extensive compositional matrix was created to study the effects of dopants on the dielectric properties of the BNT base material. Thus far, the goal of producing a material with X7R-like behavior has not been met by the systems that have been studied. Although many of the compositions have great high temperature dielectric properties, the low temperature properties have been difficult to improve. This study expanded the amount of information on the electrical properties of doped BNT. The data produced so far will be useful to refine dielectric compositional design, as well as helpful in creating a better overall understanding of the structural effects that each of the dopant systems has on the BNT base material.

Of all the samples that where measured, a few stood out as outstanding materials that did not meet the criteria for this project; however, they could potentially work for many other high temperature applications. One of the most promising samples was the Ba = 0.13, Zr = 0.07 because of its broad permittivity peak and low loss. This sample exhibits exemplary performance between the temperatures of 100° to 400°C. Figures 23 and 24 show the results for this system. The relative permittivity for this sample ranges from 3000 at 100°C to 3700 at the peak and then to 2500 at 400°C. This performance is very promising for high temperature applications that do not need the performance below room temperature.

The barium-strontium-tin doped BNT samples, shown in Figures 21 and 22, had many compositions that could be used to temperatures exceeding 450°C. The best sample (Ba = Sr = 0.15, Sn = 0.15) had a relative permittivity of 1000 at 0°C, a peak K of 2000 at 100°C, and remained above 1000 out to 450°C. The loss for this samples is near 0.1 at 0°C, which, is a little higher than desired, it drops do below 0.05 and then begins to increase around 250°C. The loss does remain below the maximum desired value of 0.1 until 400°C, which shows that this material could be used to that temperature. Again, these samples do not meet the extremely difficult criteria set forth in this project, but they are very promising for other high temperature applications with decent results to 0°C.

According to the information available from this study, the bond valence method is a useful tool for the determination of theoretical structure parameters such as bond lengths and lattice parameters. The equations are straightforward and flexible enough to fit a system with many dopants. The lattice parameters calculated by the bond valence equations are very similar to the measured values for the strontium and tin modified BNT samples. The difference between the theoretical and experimental lattice parameters must be examined further to modify the theoretical model to more closely fit the experimental values. Future work including structural refinements using neutron diffraction data will only enhance the predictive capabilities for determining the structural effects of the dopants on BNT.

The bond valence tolerance factor charts are useful for choosing compositions in a logical manner based on previous structural information. According to the charts, a tolerance factor range has been determined that describes where morphotropic phase boundary compositions should be and were found. This range can be used to predict where other A-site dopants may exhibit morphotropic phase boundary behavior. Morphotropic phase boundary systems are promising materials because they exhibit relative permittivity values that are anomalously high compared to single phase regions not near the MPB. The stability range has been determined to be between bond valence tolerance factor values of $0.965 < t < 0.975$ for A-site dopants in BNT. The results show that A-site dopants of strontium, barium, lead and potassium exhibit morphotropic phase boundary behavior for compositions within this tolerance factor range. This range is the focus of future compositions, including multi-component systems, to try and capitalize on the enhancement of the relative permittivity near the MPB.

Another significant use for the bond valence tolerance factor charts is determining a lower stability limit. A compositional limit would be useful for determining how much of a particular A or B-site dopant could be added, while still maintaining a stable perovskite structure. The stability of the structure was determined experimentally by using two methods. The first method for determining stability was to sinter the compositions with increasing dopant levels. If the dopant level was too high to form a stable structure, the pellets would not form a quality ceramic. Highly unstable structures would not sinter well so the electrical properties of the pellets could not be measured.

The other easily available method was to check the relative permittivity measurements. If the structure was stable enough to form a sintered pellet, yet unstable enough so that the electrical properties were affected, the relative permittivity results would be drastically different from the rest of the samples. These criteria were used to determine a lower stability limit for doped BNT. This value however is not as well defined as the MPB limit due to the fact that not all dopants react the same with BNT. Some may have similar physical characteristics, yet maintain a stable structure with slightly higher or lower dopant levels. The lower stability limit has a range of $0.94 < t < 0.95$. This range is shown in the bond valence tolerance factor charts in Figures 32 and 33. It should be noted that the lower stability limit is valid for both A and B-site tolerance factor values.

The tolerance factor ranges that have been determined experimentally are useful for predicting future dopant matrices because they can help focus effort in the most promising areas. The multi-component systems with compositions within the MPB range seem to show the most promising results. The existence of an MPB in the multi-component systems has yet to be confirmed.

This method is not perfected by any means, and it is still based on experimental results that are then applied to the theory. Once a better understanding of this system is obtained both experimentally and theoretically, a universal model may be created that can be used for predicting the properties of dopants in other electronic ceramic materials.

V FUTURE WORK

Future work includes more multi-component dopant systems to study the affects on the dielectric properties of BNT. This work is underway on many more multi-component systems and the results will be used to expand the knowledge of the BNT system. The bond valence tolerance factor calculations will continue to be used to choose the compositions to create a phase diagram. The most promising compositions of this and future experiments will be chosen to make larger batches to ensure that the properties remain the same with larger batches. If a composition is found that meets the goals of the project, a study will be performed to determine the best way to cast thick film tape for use in multi-layer ceramic capacitor processing. Tests will be done on the multi-layer capacitors to optimize the properties for specific electronic applications.

Neutron diffraction experiments will be performed on some compositions to relate the tolerance factor and lattice parameter calculations to the structural data. Neutron diffraction is necessary because accurate ion positions are needed to calculate the exact bond lengths and octahedral tilt angles. The experimental values will be compared to the theoretical values and the model will be modified according to the results of the neutron diffraction experiments. This knowledge will be useful to expand the understanding of the bond valence tolerance factor and its usefulness for predicting the structural and electrical properties of electronic ceramic systems.

REFERENCES

1. H. Nagata and T. Takenaka, "Lead-Free Piezoelectric Ceramics of $(Bi_{0.5}Na_{0.5})TiO_3$-$_{0.5}(Bi_2O_3$-$Sc_2O_3)$ System," *Jpn. J. Appl. Phys.,* **36** [9B] 6055-7 (1997).

2. A.J. Moulson and J.M. Herbert, *Electroceramics: Materials, Properties, Applications.,* 2nd ed. Wiley and Sons, West Sussex, England, 2003.

3. A.N. Soukhojak, H. Wang, G.W. Farrey, and Y.-M. Chiang, "Superlattice in Single Crystal Barium-Doped Sodium Bismuth Titanate," *J. Phys. Chem. Solids,* **61** [2] 301-4 (2000).

4. G.O. Jones and P.A. Thomas, "Investigation of the Structure and Phase Transitions in the Novel A-site Substituted Distorted Perovskite Compound $Na_{0.5}Bi_{0.5}TiO_3$," *Acta Crystallogr.,* **B 58** [2] 168-78 (2002).

5. P. Woodward, "Octahedral Tilting in Perovskites. I. Geometrical Considerations," *Acta Crystallogr.,* **B 53** [1] 32-43 (1997).

6. J.A. Zvirgzds, P.P. Kapostins, J.V. Zvirgzde, and T.V. Krunzina, "X-Ray Study of Phase Transitions in Ferroelectric $Na_{0.5}Bi_{0.5}TiO_3$," *Ferroelectrics,* **40** [1-2] 75-7 (1982).

7. S.-E. Park and K.S. Hong, "Variations of Structure and Dielectric Properties on Substituting A-site Cations for Sr^{2+} in $(Na_{1/2}Bi_{1/2})TiO_3$," *J. Mater. Res.,* **12** [8] 2152-7 (1997).

8. K. Sakata and Y. Masuda, "Ferroelectric and Antiferroelectric Properties of $(Na_{0.5}$ $Bi_{0.5})$ TiO_3-$SrTiO_3$ Solid Solution Ceramics," *Ferroelectrics,* **7** [1-4] 347-9 (1974).

9. S. Said, P. Marchet, T. Merle-Mejean, and J.-P. Mercurio, "Raman Spectroscopy Study of the $Na_{0.5}Bi_{0.5}TiO_3$-$PbTiO_3$ System," *Mater. Lett.,* **58** [9] 1405-9 (2004).

10. J.-K. Lee, J.Y. Yi, and K.-S. Hong, "Relationship Between Structure and Dielectric Property in $(1-x)(Na_{1/2}Bi_{1/2})TiO_3$ - $xPbZrO_3$ Ceramics," *Jpn. J. Appl. Phys., Part 1,* **40** [10] 6003-7 (2001).

11. I.P. Pronin, P.P. Syrnikov, V.A. Isupov, V.M. Egorov, N.V. Zaitseva, and A.F. Ioffe, "Peculiarities of Phase Transitions in Sodium-Bismuth Titanate," *Ferroelectrics,* **25** [1-4] 395-7 (1980).

12. P. Woodward, "Octahedral Tilting in Perovskites. II. Structure Stabilizing Forces," *Acta Crystallogr.,* **B 53** [1] 44-66 (1997).

13. G.O. Jones and P.A. Thomas, "The Tetragonal Phase of $Na_{0.5}Bi_{0.5}TiO_3$ - a New Variant of the Perovskite Structure," *Acta Crystallogr.,* **B 56** [3] 426-30 (2000).

14. M.E. Lines and A.M. Glass, *Principles and Applications of Ferroelectrics and Related Materials*. Oxford University Press, New York, 2001.

15. S.A. Sheets, A.N. Soukhojak, N. Ohashi, and Y.-M. Chiang, "Relaxor Single Crystals in the $(Bi_{1/2}Na_{1/2})_{1-x}Ba_xZr_yTi_{1-y})_3$ System Exhibiting High Electrostrictive Strain," *J. Appl. Phys.,* **90** [10] 5287-95 (2001).

16. S. Kuharuangrong, "Studies on the Dielectric Properties and the Phase Transitions of the $Bi_{0.5}Na_{0.5}TiO_3$ $PbTiO_3$"; Ph. D. Thesis. Alfred University, Alfred, NY, 1994.

17. T. Takenaka, K.-I. Maruyama, and K. Kakata, "$(Bi_{0.5}$ $Na_{0.5})TiO_3$-$BaTiO_3$ System for Lead-Free Piezoelectric Ceramics," *Jpn. J. Appl. Phys.,* **30** [9B] 2236-9 (1991).

18. H.-D. Li, C.-D. Feng, and W.-L. Yao, "Some Effects of Different Additives on Dielectric and Piezoelectric Properties of $(Bi_{1/2}Na_{1/2})TiO_3$-$BaTiO_3$ Morphotropic-Phase-Boundary Composition," *Mater. Lett.,* **58** [7-8] 1194-8 (2004).

19. J.-R. Gomah-Pettry, S. Said, P. Marchet, and J.-P. Mercurio, "Sodium-Bismuth Titanate Based Lead-Free Ferroelectric Materials," *J. Eur. Ceram. Soc.,* **24** [6] 1165-9 (2004).

20. J. Suchanicz, M.G. Gavshin, A.Y. Kudzin, and C. Kus, "Dielectric Properties of $(Na_{0.5}Bi_{0.5})_{1-x}$ Me_xTiO_3 Ceramics near Morphotropic Phase Boundary," *J. Mater. Sci.,* **36** [8] 1981-5 (2001).

21. S. Said and J.-P. Mercurio, "Relaxor Behavior of Low Lead and Lead Free Ferroelectric Ceramics of the $Na_{0.5}Bi_{0.5}TiO_3$-$PbTiO_3$ and $Na_{0.5}Bi_{0.5}TiO_3$-$K_{0.5}Bi_{0.5}TiO_3$ Systems," *J. Eur. Ceram. Soc.,* **21** [10-11] 1333-6 (2001).

22. S. Kuharuangrong, "Effect of La and K on The Microstructure and Dielectric Properties of $Bi_{0.5}Na_{0.5}TiO_3$-$PbTiO_3$," *J. Mater. Sci.,* **36** [7] 1727-33 (2001).

23. H. Nagata, M. Yoshida, Y. Makiuchi, and T. Takenaka, "Large Piezoelectric Constant and High Curie Temperature of Lead-Free Piezoelectric Ceramic Ternary System Based on Bismuth Sodium Titanate-Bismuth Potassium Titanate-Barium Titanate Near the Morphotropic Phase Boundary," *Jpn. J. Appl. Phys.,* **42** [12] 7401-3 (2003).

24. A. Sasaki, T. Chiba, Y. Mamiya, and E. Otsuki, "Dielectric and Piezoelectric Properties of $(Bi_{0.5}Na_{0.5})TiO_3$-$(Bi_{0.5}K_{0.5})TiO_3$ Systems," *Jpn. J. Appl. Phys., Part 1,* **38** [9B] 5564-7 (1999).

25. H. Ishii, H. Nagata, and T. Takenaka, "Morphotropic Phase Boundary and Electrical Properties of Bisumuth SodiumTitanate - Potassium Niobate Solid-Solution Ceramics," *Jpn. J. Appl. Phys., Part 1,* **40** [9 B] 5660-3 (2001).

26. H. Nagata and T. Takenaka, "Lead-Free Piezoelectric Ceramics of $(Bi_{0.5}Na_{0.5})TiO_3$-$KNbO_{3-0.5}(Bi_2O_3$-$Sc_2)_3)$ System," *Jpn. J. Appl. Phys.,* **37** [9B] 5311-4 (1998).

27. A. Herabut and A. Safari, "Processing and Electromechanical Properties of $(Bi_{0.5}Na_{0.5})_{(1-1.5x)}La_xTiO_3$ Ceramics," *J. Am. Ceram. Soc.,* **80** [12] 2954-8 (1997).

28. J.Y. Yi, J.-K. Lee, and K.-S. Hong, "Dependence of the Microstructure and the Electrical Properties of Lanthanum-Substituted $(Na_{1/2}Bi_{1/2})TiO_3$ on Cation Vacancies," *J. Am. Ceram. Soc.,* **85** [12] 3004-10 (2002).

29. M. Aparna, T. Bhimasankaram, G.S. Kumar, and G. Prasad, "Synthesis and Characterization of Lanthanum Doped Sodium Bismuth Titanate," *Modern Physics Letters,* **B 16** [26] 1007-19 (2002).

30. X.X. Wang, K.W. Kwok, X.G. Tang, H.L.W. Chan, and C.L. Choy, "Electromechanical Properties and Dielectric Behavior of $(Bi_{1/2}Na_{1/2})_{(1-1.5x)}Bi_xTiO_3$ Lead-Free Piezoelectric Ceramics," *Solid State Commun.,* **129** [5] 319-23 (2004).

31. H. Nagata and T. Takenaka, "Additive Effects on Electrical Properties of $(Bi_{1/2}Na_{1/2})TiO_3$ Ferroelectric Ceramics," *J. Eur. Ceram. Soc.,* **21** [10-11] 1299-302 (2001).

32. J.P. Attfield, "'A' Cation Control of Perovskite Properties," *Cryst. Eng.,* **5** [3-4] 427-38 (2002).

33. C.A. Randall, A.S. Bhalla, T.R. Shrout, and L.E. Cross, "Classification and Consequences of Complex Lead Perovskite Ferroelectrics with Regard to B-site Cation Order," *J. Mater. Res.,* **5** [4] 829-34 (1990).

34. W.A. Schulze, Thesis Discussion, Alfred University, 2002-2004.

35. Y.J. Feng, Z. Xu, and X. Yao, "Effect of Sn Doping on the Phase Transition Behaviors of Antiferroelectric Lead Zirconate Titanate," *Mater. Sci. Eng.,* **B 99** [1-3] 499-501 (2003).

36. B. Jaffe, W.R.C. Jr., and H. Jaffe, *Piezoelectric Ceramics*. Academic Press Limited, New York, 1971.

37. S. Kuharuangrong and W. Schulze, "Characterization of $Bi_{0.5}Na_{0.5}TiO_3$-$PbTiO_3$ Dielectric Materials," *J. Am. Ceram. Soc.,* **79** [5] 1273-80 (1996).

38. I.D. Brown, The Chemical Bond in Inorganic Chemistry: The Bond Valence Model. Oxford University Press, New York, 2002.

39. I.D. Brown and D. Altermatt, "Bond-Valence Parameters Obtained from a Systematic Analysis of the Inorganic Crystal Structure Database," *Acta Crystallogr.,* **B41** [4] 244-7 (1985).

40. M. Kunz and I.D. Brown, "Out-of-Center Distortions around Octahedrally Coordinated d^0 Transition Metals," *J. Solid State Chem.,* **115** [2] 395-406 (1995).

41. I.D. Brown, A. Dabkowski, and A. McCleary, "Thermal Expansion of Chemical Bonds," *Acta Crystallogr.,* **B53** [5] 750-61 (1997).

42. N. Thomas, "The Compositional Dependence of Octahedral Tilting in Orthorhombic and Tetragonal Perovskites," *Acta Crystallogr.,* **B 52** [1] 16-31 (1996).

43. A.M. Glazer, "Simple Ways of Determining Perovskite Structures," *Acta Crystallogr.,* **A31** [6] 756-62 (1975).

44. N.W. Thomas, "A Re-examination of the Relationship Between Lattice Strain, Octahedral Tilt Angle and Octahedral Strain in Rhombohedral Perovskites," *Acta Crystallogr.,* **B52** [6] 954-60 (1996).

45. C.J. Howard and H.T. Stokes, "Group-Theoretical Analysis of Octahedral Tilting in Perovskites," *Acta Crystallogr.,* **B54** [6] 782-9 (1998).

46. C.N.W. Darlington, "Normal-Mode analysis of the Structures of Perovskites with Tilted Octahedra," *Acta Crystallogr.,* **A58** [1] 66-71 (2002).

47. Y.A. Abramov, V.G. Tsirelson, V.E. Zavodnik, S.A. Ivanov, and I.D. Brown, "The Chemical Bond and Atomic Displacements in $SrTiO_3$ from X-ray Diffraction Analysis," *Acta Crystallogr.,* **B 51** [6] 942-51 (1995).

48. N.W. Thomas, "Beyond the Tolerance Factor: Harnessing X-ray and Neutron Diffraction Data for the Compositional Design of Perovskite Ceramics," *Br. Ceram. Trans.,* **96** [1] 7-15 (1997).

49. N.W. Thomas, "Crystal Structure-Physical Property Relationships in Perovskites," *Acta Crystallogr.,* **B45** [4] 337-44 (1989).

50. N.W. Thomas, "A New Parameterization for Investigating Relationships Between Chemical Composition and Crystal Structure in Layered ABO_3 Ceramics," *Acta Crystallogr.,* **B47** [5] 597-608 (1991).

51. N. Thomas, "A New Global Parameterization of Perovskite Structures," *Acta Crystallogr.,* **B 54** [5] 585-99 (1998).

52. N.W. Thomas and A. Beitollahi, "Inter-relationship of Octahedral Geometry, Polyhedral Volume Ratio and Ferroelectric Properties in Rhombohedral Perovskites," *Acta Crystallogr.,* **B 50** [5] 549-60 (1994).

53. J.S. Reed, *Principles of Ceramics Processing,* 2nd ed. John Wiley & Sons, New York, 1995.

54. M.S. Haluska and S.T. Misture, "Crystal Structure Refinements of the Three-Layer Aurivillius Ceramics $Bi_2Sr_{2-x}A_xNb_2TiO_{12}$ (A=Ca,Ba, x=0,0.5,1) Using Combined X-ray and Neutron Powder Diffraction," *J. Solid State Chem.,* **177** [6] 1965-75 (2004).

55. B.H. Toby, "EXPGUI, a Graphical User Interface for GSAS," *J. Appl. Crystallogr.,* **34** [2] 210-3 (2001).

56. A.C. Larson and R.B.V. Dreele, General Structure Analysis System (GSAS), [Computer Program] Los Alamos National Laboratory, Report LAUR 86-748, 1994.

57. L.B. McCusker, R.B.V. Dreele, D.E. Cox, D. Louer, and P. Scardi, "Rietveld Refinement Guidelines," *J. Appl. Crystallogr.,* **32** [1] 36-50 (1999).

58. I. Brown, "Predicting Bond Lengths in Inorganic Crystals," *Acta Crystallogr.,* **B33** [5] 1305-10 (1977).

59. I. Brown, "What Factors Determine Cation Coordination Numbers?," *Acta Crystallogr.,* **B44** [6] 545-53 (1988).

60. I. Brown, "Chemical and Steric Constraints in Inorganic Solids," *Acta Crystallogr.,* **B48** [5] 553-72 (1992).

61. I.D. Brown, "Internal Strain in Perovskite Related Materials," pp. 471-83 in *Chemistry of Electronic Ceramic Materials*. Edited by P. K. Davies and R. S. Roth. Technomic Publishing Company, Lancaster, PA, 1990.

62. I.D. Brown, "A Determination of the Oxidation States and Internal Stresses in $Ba_2YCu_3O_x$, x = 6-7 Using Bond Valences," *J. Solid State Chem.,* **82** [1] 122-31 (1989).

APPENDICES

A. Firing Profiles Used for this Study

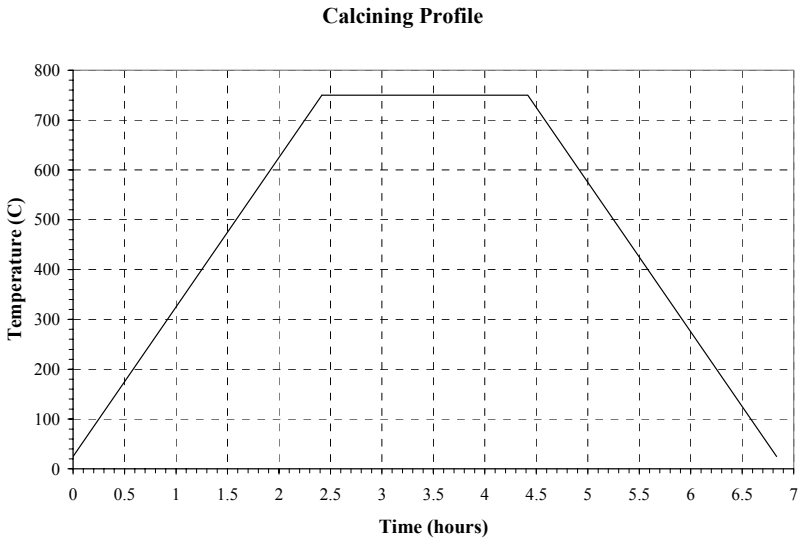

Figure 39. Typical firing profile used to calcine the powders.

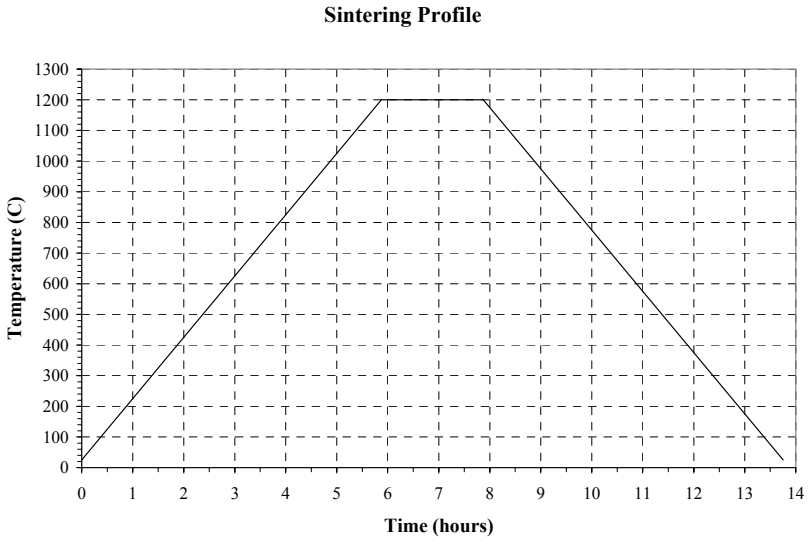

Figure 40. Typical firing profile used to sinter the pellets.

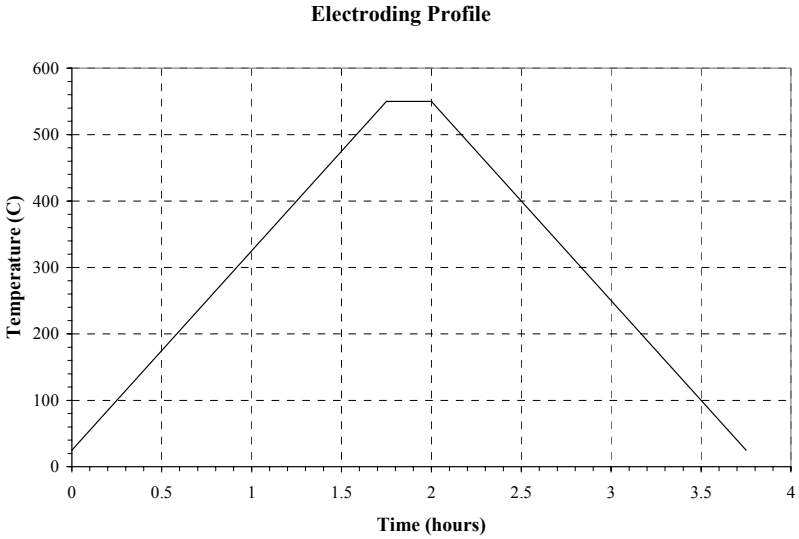

Figure 41. Firing profile used to sinter the electrode material on the pellets.

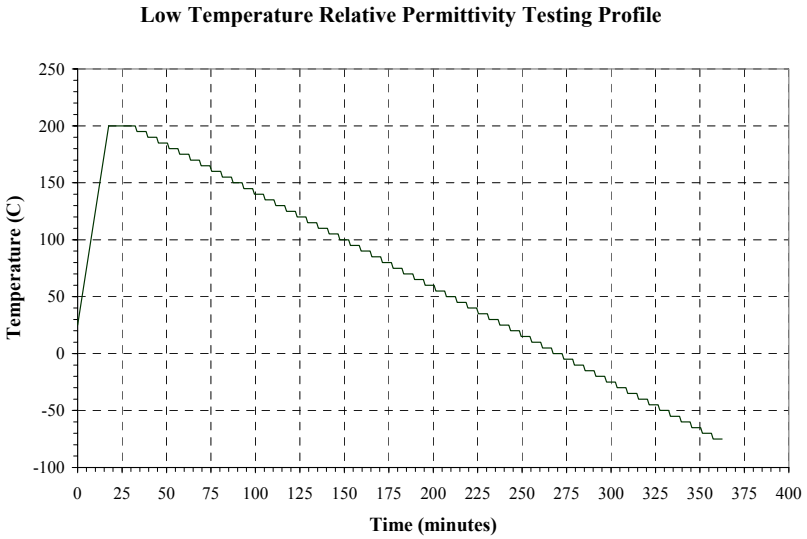

Figure 42. Heating profile used for the low temperature relative permittivity measurements.

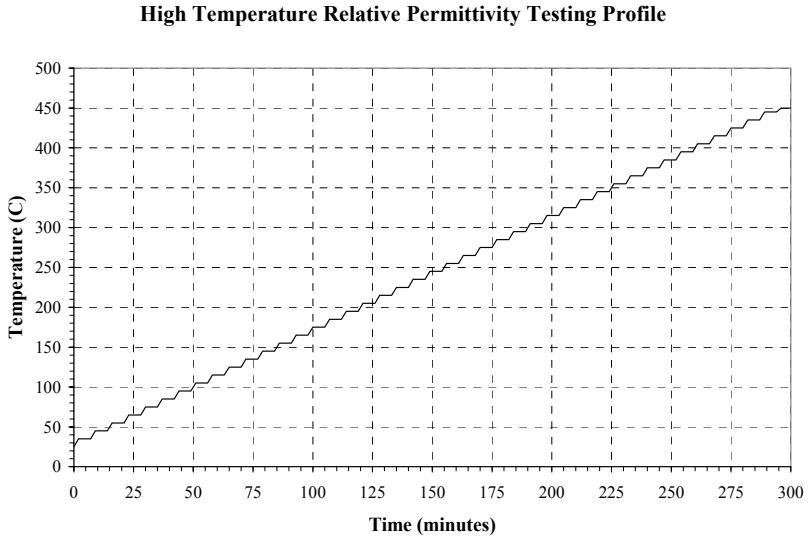

Figure 43. Heating profile used for the high temperature relative permittivity measurements.

B. X-ray Diffraction Pattern of Pure Bismuth Sodium Titanate

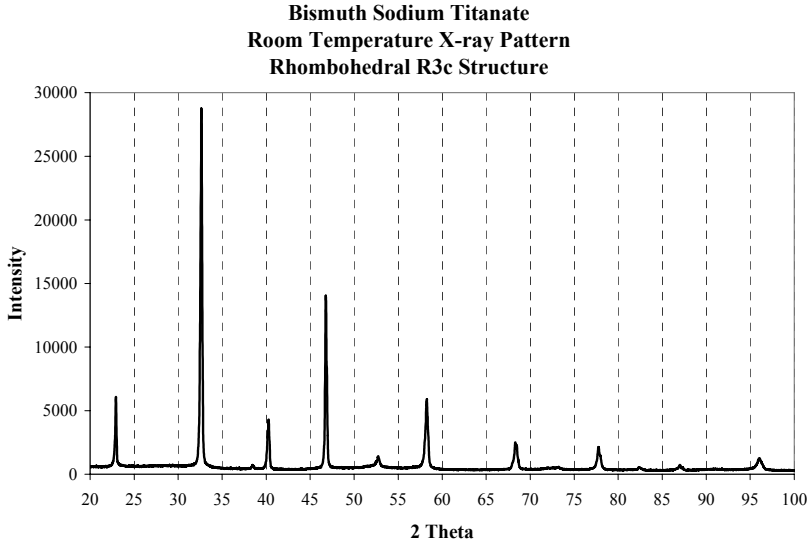

Figure 44. X-ray pattern of 100% BNT in the rhombohedral R3c structure.

C. GSAS/EXPGUI Rietveld Refinement Procedure

1. For x-ray data, insert profile type 3, LX = 8, LY = 20.
2. Histogram Tab: select cosine Fourier, 3 terms.
3. Histogram Tab: Fraction should be set to 0.5

4. Initial refinement should be base pattern with only scale and background refined.
5. Refine lattice parameters, turn off.
6. Refine LY.
7. Turn off LY, turn on LX and refine.
8. Turn off LX, turn on SHFT and refine.
9. Turn off SHFT, turn on MD preferred orientation (MD PO) and refine.
10. Turn off MD PO, turn on POLA in the Histogram tab and refine.
11. Turn off POLA, turn on S/L in the Profile tab and refine.
    a. if S/L goes to .005, reset to .015
12. Turn off S/L, add two histogram terms and refine.
13. Check pattern by choosing the powplot function. Exclude unnecessary regions as needed. For example, low angle background spike, regions without any significant peaks. This can be done earlier if needed.
14. Re refine LX and LY simultaneously.
15. Re-refine the lattice parameters.
16. Perform these steps until the refinement has progressed to a point where further refinements are no longer making significant changes to the parameters.
17. Follow the guidelines in the literature for refinements and program functions.
18. SAVE.[55-57]

D. EIA Reference Ranges for Capacitor Materials

Table IV. EIA Reference Ranges for Capacitor Materials.

Low Temp. Limit:	High Temp. Limit:	Capacitance Change over Range:
X -55C	4 +65C	A ± 1.0%
Y -30C	5 +85C	B ± 1.5%
Z +10C	6 +105C	C ± 2.2%
	7 +125C	D ± 3.3%
	8 +150C	E ± 4.7%
	9 +200C	F ± 7.5%
		P ± 10%
		R ± 15%
		S ± 22%
		T +22% -33%
		U +22% -56%
		V +22% -82%

E. Structural Representations of BNT Structures in Various Orientations

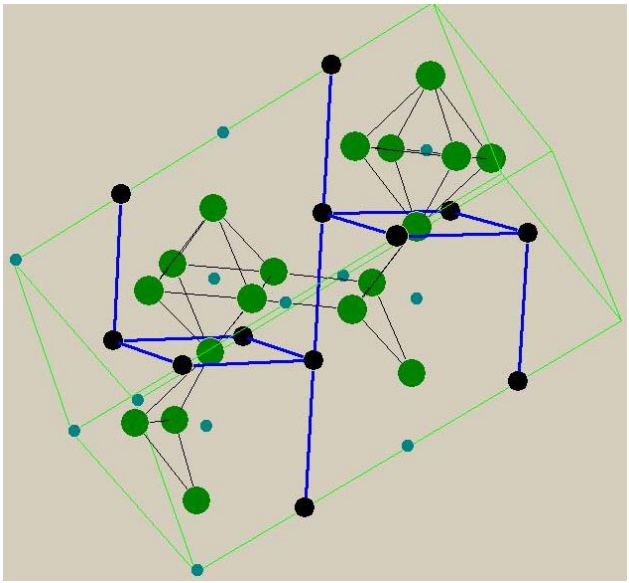

Figure 45. This figure shows the rhombohedral structure of pure BNT. The figure shows that the oxygen octahedra are tilted and rotated in the $a^-a^-a^-$ tilt system.

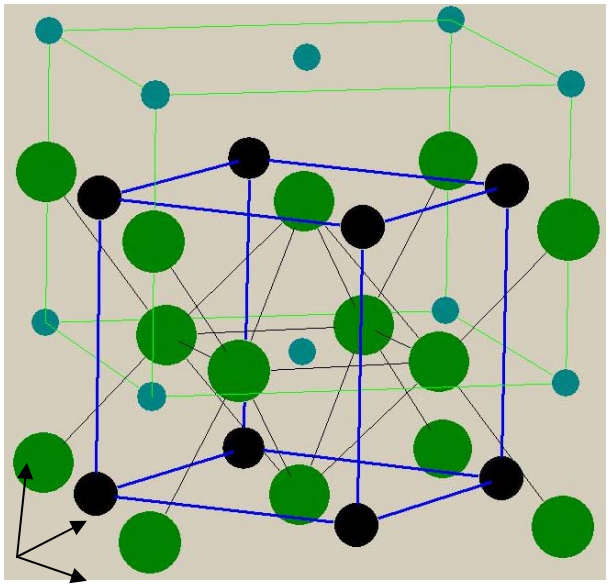

Figure 46. This figure shows the tetragonal phase of pure BNT with the a-b axes in the horizontal direction and the c-axis in the vertical direction. The tetragonal cell is denoted by the cell in the background and the cell in the foreground denotes the pseudocubic unit cell.

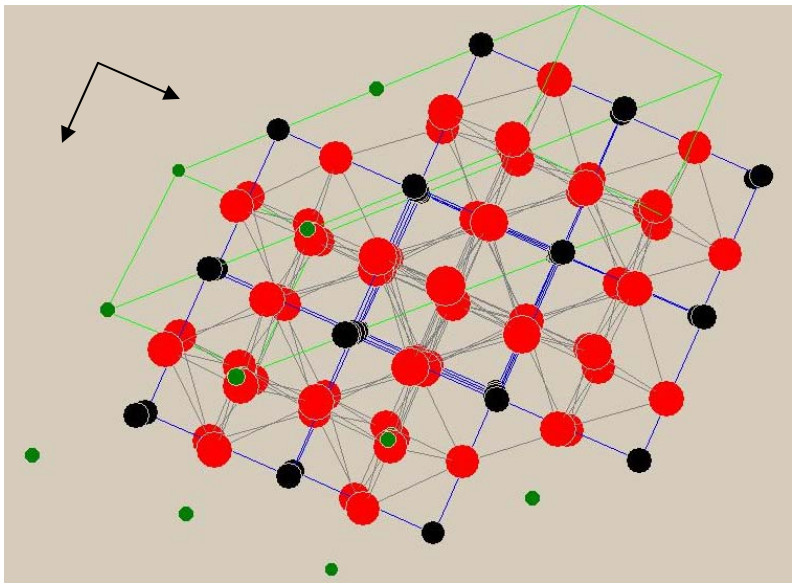

Figure 47. This figure shows the $a^{-}a^{-}a^{-}$ tilt system in rhombohedral BNT with the arrows denoting the a-b axes. The large red circles are the oxygen anions and the tilt system can be seen by the way that the oxygen anions are displaced in opposite directions from layer to layer.

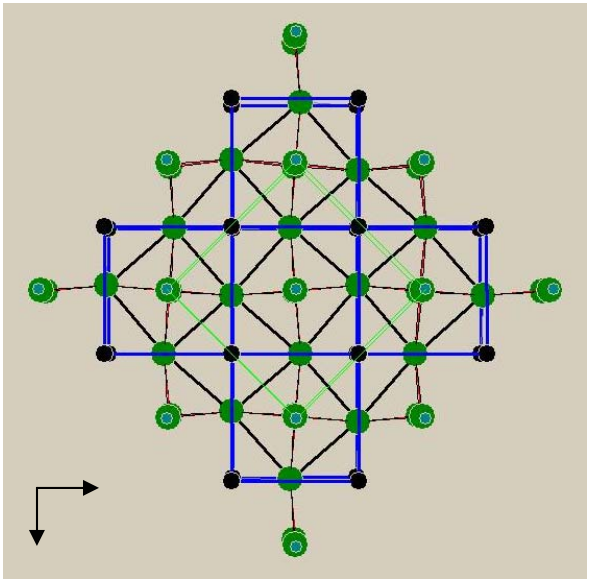

Figure 48. This figure shows the $a^{0}a^{0}a^{-}$ tilt system in the tetragonal phase of pure BNT. The figure is oriented with the c-axis pointing out of the paper and the arrows denoting the a-b axes respectively. The oxygen octahedra are rotated about the c-axis of the structure. Adjacent octahedra are rotated in opposite directions.

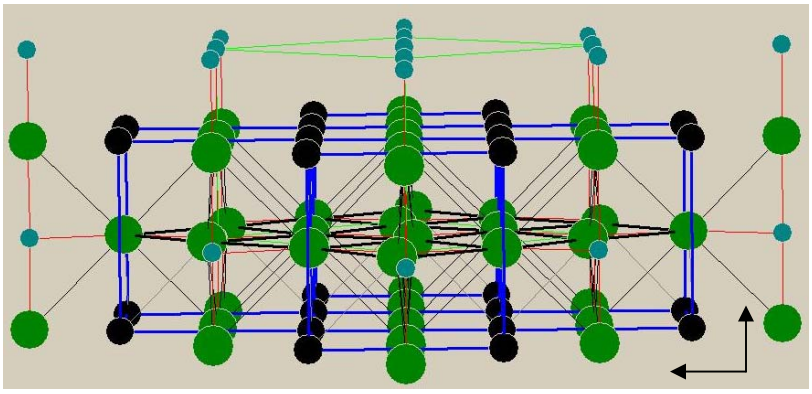

Figure 49. This figure shows how the oxygen anions are displaced from the octahedral rotation in Figure 49 above. In the figure, the c-axis is in the vertical direction and the a-b axes in the horizontal directions.